REPORT DOCUMENTATION PAGE

Form Approved
OMB No. 074-0188

1. AGENCY USE ONLY (Leave blank)	2. REPORT DATE	3. REPORT TYPE AND DATES COVERED
	12/0/000	Final. 15 AUG 94 – 14 AUG 98

4. TITLE AND SUBTITLE
Advanced Optical Diagnostics of Hgih Density Etching Plasmas

5. FUNDING NUMBERS
DAA04-94-G-0340

6. AUTHOR(S)
N.J. Ianno and P.F. Williams

7. PERFORMING ORGANIZATION NAME(S) AND ADDRESS(ES)
University of Nebraska

8. PERFORMING ORGANIZATION REPORT NUMBER

9. SPONSORING / MONITORING AGENCY NAME(S) AND ADDRESS(ES)
U.S. Army Research Office
PO Box 12211
Reserch Triangle Park, NC 27709-2211

10. SPONSORING / MONITORING AGENCY REPORT NUMBER
ARO 33636.1-RT-DPS

11. SUPPLEMENTARY NOTES
The views, opinions, and or findings in this report are those of the authors and should not be construed as an official Department of the Army position, policy, or decision, unless so designated by other documentation.

12a. DISTRIBUTION / AVAILABILITY STATEMENT
Approved for Public Release, distribution unlimited

12b. DISTRIBUTION CODE

13. ABSTRACT (Maximum 200 Words)

The purpose of this work was to investigate the use of in-situ spectroscopic ellipsometry as a means to control the etching of III-V semiconductors and in particular an AlGaAs/GaAs heterostructure used to form the emitter/base junction of a heterojunction bipolar transistor (HBT) used in high frequency circuits employed in Air Force communications. The specific objective was to use in-situ SE to monitor the etching of the AlGaAs emitter layer and stop to within a few nanometers of the GaAs base layer. Toward this end, an Electron Cyclotron Resonance (ECR) microwave plasma system and custom built stainless steel bell jar were used to construct an etch tool. The ECR microwave plasma is a low pressure, high density plasma source capable of producing highly anisotropic etch profiles. The ellipsometer used was a J.A. Woollam Co. model M-44. The M-44 is a 44 wavelength ellipsometer operating in the visible region from ~400-800 nm.

20010222 045

14. SUBJECT TERMS			15. NUMBER OF PAGES
			16. PRICE CODE
17. SECURITY CLASSIFICATION OF REPORT	18. SECURITY CLASSIFICATION OF THIS PAGE	19. SECURITY CLASSIFICATION OF ABSTRACT	20. LIMITATION OF ABSTRACT
Unlcassified	unclassified	unclassified	UL

INTRODUCTION

Accurate endpoint detection, overall process monitoring and control of the etching of multilayer stacks are essential for reproducible fabrication of III-V semiconductor devices. Ellipsometry is a nondestructive, optical technique that can accurately determine the thickness of III-V semiconductor films. When combined with the computational speed of a personal computer, ellipsometry can provide information about layer thickness and uniformity during the plasma etching of III-V materials. Real time monitoring of layer thickness allows for end point detection and termination of the etch at a desired point. For multilayered photoresist (dielectric) structures, *in-situ* ellipsometry can be used for etch rate control and end point detection, exhibiting complete control of the etch process.

The purpose of this work was to investigate the use of *in-situ* spectroscopic ellipsometry as a means to control the etching of III-V semiconductors and in particular an AlGaAs/GaAs heterostructure used to form the emitter/base junction of a heterojunction bipolar transistor (HBT) used in high frequency circuits employed in Air Force communications. The specific objective was to use *in-situ* SE to monitor the etching of the AlGaAs emitter layer and stop to within a few nanometers of the GaAs base layer. Toward this end, an Electron Cyclotron Resonance (ECR) microwave plasma system and custom built stainless steel bell jar were used to construct an etch tool. The ECR microwave plasma is a low pressure, high density plasma source capable of producing highly anisotropic etch profiles. The ellipsometer used was a J.A.

Woollam Co. model M-44. The M-44 is a 44 wavelength ellipsometer operating in the visible region from ~400-800 nm.

To become familiar with the etching characteristics of the ECR reactor, and to test the performance of the M-44 with this system, etching studies were performed using diamond like carbon (DLC) films on silicon substrates in an oxygen plasma. The optical constants of DLC are well known, therefore the thickness of DLC films could be modeled accurately with ellipsometry.[1] Diamond like carbon films were fabricated at UNL, so this was a convenient and inexpensive material system to use for testing purposes.[2] Etching uniformity and etch rate were investigated as a function of gas flow rate, pressure, microwave power, and rf induced dc bias of the sample. Results of these experiments revealed that increased uniformity was achieved at higher pressures and with rf biasing of the sample.[2] Using the information obtained from the DLC etching experiments, etching studies of GaAs were undertaken as the next step to controlling the etch process. It is at this point that the work presented in this thesis was begun.

The body of this thesis consists of four main chapters. Chapter 1 will be a brief discussion of the ECR microwave plasma and the experimental apparatus. The subject of Chapter 2 is the empirical modeling of GaAs etching using DISCOVERY™ and OPTIMIZATION™ experimental design and analysis software from Int'l Qual-Tech, Ltd. These software packages were used to develop a model equation for the etch rate of GaAs by statistical analysis of a small number of etching trials. The resulting equation predicts the etch rate for a given level of the process variables identified as significant to this "response". These variables were microwave power in watts, rf induced dc bias in

volts, and operating pressure in millitorr. The experimental design of the trials was a Face Centered Central Composite.[3]

A $CH_4/Ar/H_2$ gas mix was used for the etching of GaAs in the etch rate modeling studies.[4] Ellipsometric analysis of these samples identified the presence of a thin etch-induced surface damage layer. A set of experiments were performed using pure H_2, pure Ar, and the $CH_4/Ar/H_2$ mix to etch GaAs in order to help identify the cause and form of this damage. *Ex-situ* ellipsometry was used to analyze these samples to determine the specific details of the damage. *Ex-situ* ellipsometry was also used for analysis of similar damage seen in the etching of AlGaAs. Since considerable time was spent studying the damage, and because it was necessary to model this layer ellipsometrically, Chapter 3 will be devoted to this topic. A brief overview of ellipsometry will also be included in this chapter.

Chapter 4 deals with the attempt to control the etching of an AlGaAs/GaAs heterostructure using *in-situ* spectroscopic ellipsometry as a feedback input. The feedback provided by the ellipsometer is the thickness of the top layer(s) at discrete times during the etch. This feedback "signal" is not continuous, but rather has a frequency dependent on the time between measurements. The frequency of the measurements is user selectable and is generally chosen according to the etch rate; i.e., the faster the etch rate the more frequent the measurements and the slower the etch rate the less frequent the measurements. The M-44 is capable of making measurements at 44 wavelengths simultaneously in 40 milliseconds.

The calculated model fit parameters and time of the corresponding ψ and Δ measurements are generated in the ellipsometer software W.V.A.S.E.™[5] Once the fit

parameters are calculated, the values and the time (time=0 at the start of the etch) are automatically passed to a control algorithm written in Microsoft Visual Basic (VB). The passing of this data invokes the VB program by generating an "event procedure" within the application. The VB program thus activated, then processes this data and adjusts the system accordingly to achieve the desired results. A "result" of interest for an etching process is endpoint detection and termination of the etch once the endpoint is reached. For some material systems, AlGaAs/GaAs included, ellipsometry can lose accuracy once the film becomes very thin (on the order of a few tens of nanometers for AlGaAs/GaAs). This presents an obstacle when trying to accurately etch a layer down to this thickness range. To overcome this hurdle, a feed forward technique has been implemented whereby an accurate etch rate calculation is used to project to the end of the etch. From an etch rate calculation while the film is sufficiently thick to yield accurate data, a time to continue the etch can be obtained. The endpoint is then determined by a counter and not by the ellipsometer directly. This feed forward projection has been successfully implemented for the etching of the AlGaAs/GaAs heterostructure.

The development and testing of the control system was done using model 1400-27 and PMGI photoresist materials on silicon. These samples were provided by the Air Force for reasons other than etch control, but turned out to be an excellent, low cost method to debug the system. It was found that these materials could be accurately modeled ellipsometrically during etching down to a thickness on the order of ~30Å. It was possible therefore to track the thickness of the top layer of a two layer photoresist sample down to the interface and continue to track the bottom layer as it began to etch. The extremely accurate modeling of the photoresists allowed for etch rate control of

these materials whereby the control algorithm adjusted the rf bias to achieve a preselected target rate.

A few significant problems were encountered on the road to controlling the etch process that deserve mention here. The damage created by the $CH_4/Ar/H_2$ etching of AlGaAs complicated the modeling of this material. This damage was a somewhat unexpected but inherent consequence of the physical nature of the etch and, as mentioned earlier, will be discussed fully in Chapter 3. The second, and perhaps most troublesome difficulty, was the nonuniform etching of AlGaAs in the ECR system. The DLC etching studies for uniformity showed that an approximately 80% uniform etch across a distance of 4 cm was possible.[2] With AlGaAs (and GaAs) however, etch profiles were obtained with significant nonuniformity over distances as small as 0.5 cm. The severity of the nonuniformity was eventually reduced significantly, but at the price of a substantially reduced etch rate. This issue will be discussed along with the control implementation in Chapter 4. Following the final chapter, this thesis will conclude with a summary of the work presented.

1. The ECR System

1.1 The ECR Plasma

The Electron Cyclotron Resonance (ECR) microwave plasma is a low pressure (<0.5 Torr) plasma generated by coupling microwave energy to the electron gas in the presence of a static magnetic field.[6] The cyclotron frequency of an electron in a magnetic field is given by $\omega_c = eB/m$ where e is the charge on the electron, B is the magnetic field strength, and m is the mass of the electron. The resonance condition is reached in ECR "layers" (typically < 1 mm thick) where **E** is perpendicular to **B** and the input microwave frequency is equal to the cyclotron frequency, ω_c. Under low pressure conditions, where the electron collision frequency is much less than the cyclotron frequency, an electron can experience many oscillations in phase with the electric field while in the ECR layer and therefore large amounts of energy can be coupled at relatively low electric field intensities. The amount of energy coupled to the electron gas is therefore very dependent on the pressure and scattering cross section of the ion/neutral gas. In the ECR layer the electron velocity perpendicular to the magnetic field line increases, giving the electron a forward, outward spiraling motion as shown in Figure 1-1. The energized electron leaves the ECR layer and makes elastic and inelastic collisions and thus excites, ionizes, and disassociates ions and neutrals.[6]

1.2 Experimental Apparatus

A diagram of the etching system is given in Figure 1-2. The chamber is pumped by a Leybold 600 l/s turbo pump with a base pressure of typically 7×10^{-7} Torr. The ECR system is a Microscience 900, magnetic mirror type with electromagnets and a 1000 watt, 2.45 GigaHertz (B = 875 Gauss) power source. The M-44 mounts on optical

ports made of strain-free quartz windows. The chamber was custom built such that the incident probe beam makes a nominal angle of 75° to the surface normal. (This is very near the optimum angle of incidence for semiconductors.) The sample stage is translatable and RF biased by a 13.56 MegaHertz, 500 watt (max) power supply employing an automatic matching network. The sample holder is an approximately 3.5 mm thick by 7 cm diameter copper disk with two windings of 0.25 inch copper tubing soldered to the backside for water cooling. The samples were mounted on the holder using WATLUBE (a heat transfer agent) for surface contact and silver paint around the edges for good adhesion and electrical contact. All samples (except where noted) used for etching in this work were ~ 1 x 2 cm pieces cut from wafers. Gas metering was accomplished using an MKS flow control system with the CH_4 injected into the gas ring and all other gases administered through gas input 1. A picture of the etching system is given in Figure 1-3.

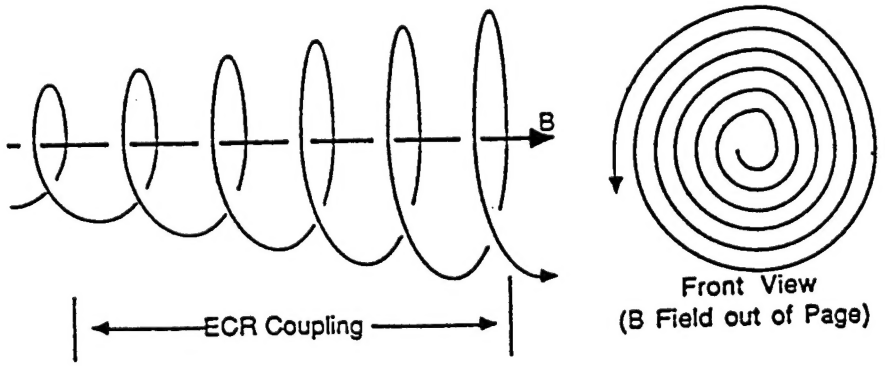

Figure 1-1. Motion of an electron in static magnetic and oscillating electric fields.

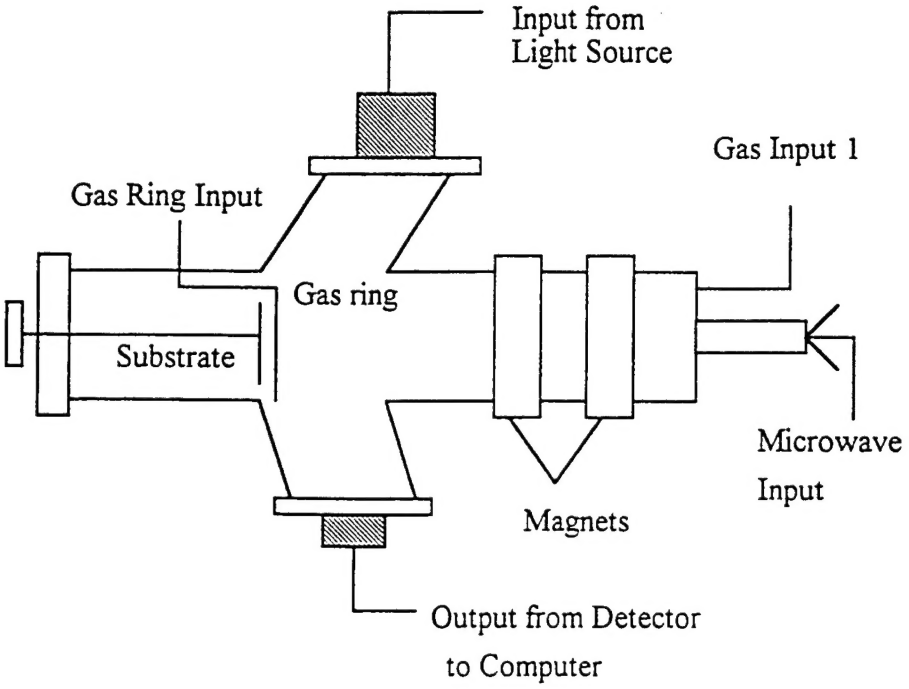

Figure 1-2. Diagram of the ECR etching system (top view).

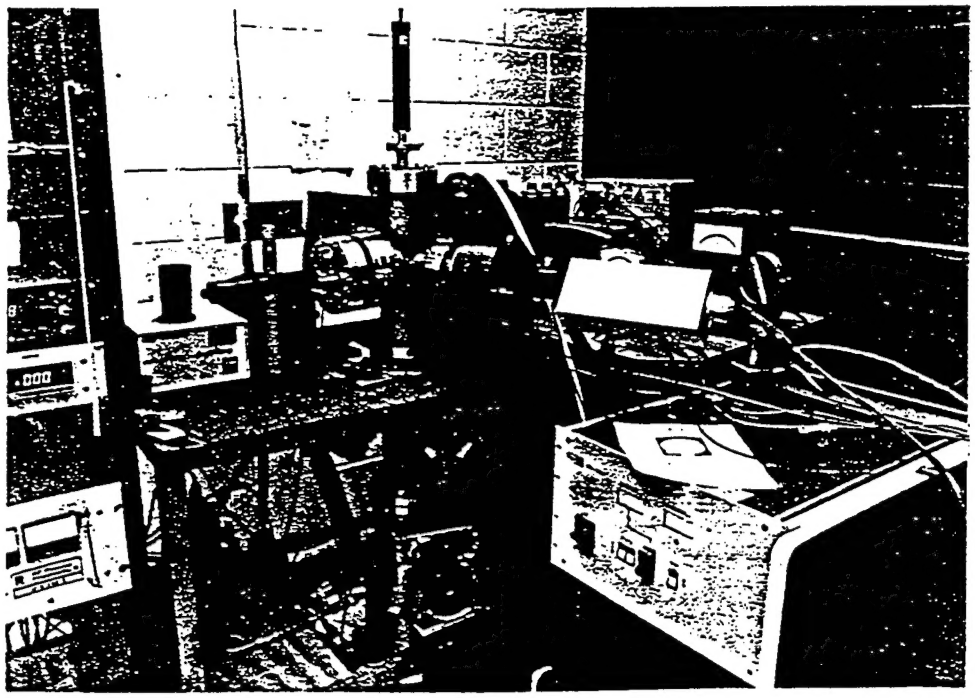

Figure 1-3. Picture of the ECR etching system.

2. Empirical Modeling of GaAs ECR Etching

If the Discovery-generated model sufficiently fit the screening was not required. The usual approach to experimentation is the "one-variable-at-a-time" method. In this method, the optimum level for each variable is determined by varying one parameter while all others are held constant. The optimum variable level is that which gives the optimum in the measured response. The measured response could be, for example, the amount of product from a chemical reaction. If the amount of product obtained depends on the temperature at which the reaction is carried out, then the optimum temperature level is that which gives the largest amount of product.

The "one-variable-at-a-time" method has disadvantages in that a large number of trials are usually required and the variable interactions cannot be estimated. For some processes, variable interaction can be significant to the response , thus using the "one-variable-at-a-time" method can sometimes lead to an incorrect determination of the true optimum levels. A more efficient approach is to design the experiments such that more than one parameter is allowed to vary. The "design of experiments" approach reduces the number of trials required and allows for the estimation of variable interactions.[7]

There are three sources of difficulty that an empirical (or statistical) method must account for to yield reliable results. First, variation produced by known or unknown sources (experimental error) must be minimized and analysis should give a measure of the probability that an effect is real and not a result of experimental error. Secondly, there can be correlation between two variables which can be confused with causation. For example, in an experiment it is observed that an increase in the variables X and Y is associated with an increase in a third factor, Z. An increase in X (or Y), it would appear,

could just as well be the result of an increase in Y (or X), but the "truth" of the matter is that only an increase in Z causes an increase in X and Y. This difficulty is known as "confusion of correlation with causation."[7] The third difficulty lies in the complexity of the variable effects on the measured response. Any nonlinearity in a variable effect or any interaction between variables can make it more difficult to determine the actual relationship between the experimental variables and the response. All three of these possibilities can lead to erroneous results and misinterpretation of the true state of the subject under investigation.[7] By carefully designing the experiments using proven techniques, the possibility of error can be greatly reduced and the probability of finding the true nature of the system can be significantly increased. Discovery and Optimization offer experimental designs to minimize the chance of error and determine the variable effects and interactions in a minimum number of trials.

This chapter describes the work done using Discovery and Optimization experimental design and analysis software from Int'l Qual-Tech, Ltd. to model the etch rate of bulk GaAs in a $CH_4/Ar/H_2$ ECR plasma as a function of microwave power, rf induced dc bias, and pressure. These three parameters are the process variables and the etch rate is the measured response or outcome of the experiment. Other variables could have been investigated, however previous studies have shown that the etch rate depends primarily on these three variables.[4] The flow ratio of the CH_4 and H_2 is critical to achieve any etching (due to the gas chemistry) and a CH_4: H_2 ratio of ~0.2-0.4 is reported to be necessary for polymer free etching.[4] Therefore, a fixed $CH_4/Ar/ H_2$ flow ratio of 3.3/5/10 sccm was used for all bulk GaAs experiments described in this chapter.

2.1 Discovery and Optimization Software

Discovery and Optimization are two separate but complementary experimental design and analysis software packages. In a typical application, when the "critical" variables (those variables which have a significant affect on the response) are not known, it is desirable to perform an initial, small number of experiments to screen for the critical variables. Once these variables are identified, a more extensive, "complete" set of experiments can be conducted to determine the response (etch rate) as a function of the process variables (microwave power, bias, pressure). Discovery is used to design and analyze the initial experiments while Optimization is utilized to design and analyze the final experiments. By using this two step process, efficiency is maximized by minimizing time and monetary expenditures. Many of the experimental designs offered by Discovery can be used in the Optimization experiments to further increase the efficiency by reducing the total number of runs required.

The type of Discovery design used depends on the number of variables to be investigated, but the common feature of all designs is performing experiments at two levels of each variable. If n variables are included, then for a "full factorial" design, 2^n trials are needed.[7] The number of trials therefore increases exponentially with the number of variables for this design. For large n, it is more appropriate to use a "fractional factorial" design or one of the more sophisticated designs offered by Discovery.[8] For the present case with only three variables, the "full factorial" design is the best choice since only 2^3 or eight runs are required.

The Discovery experiments not only screen for the critical variables but also "gauge" the nonlinearity in the response. Any nonlinearity is determined by augmenting the eight factorial runs with a trial at the middle level of each variable, or a so called

"center point run." After the nine total runs are completed, Discovery is used to analyze the results and construct a linear mathematical model that best fits the data. (The linear model is generated using only the eight factorial trials.) The measured response at the center point is then compared to the model predicted response at the center point and the difference between the two values gives an indication of the nonlinearity. If the difference is very small, then the relationship may be linear. However, if there is a substantial difference, as in the present case, then additional experiments are needed (Optimization) to model the data.

Optimization experimental designs include trials at three to five levels of each variable to develop a nonlinear model of the process response. As with Discovery, the type of design depends on the number of variables. The designs offered by Optimization allow at least partial or, in this case, complete inclusion of the experiments performed in the Discovery design. The 2^3 full factorial experiments in Discovery can be thought of as a cube with each trial represented by a corner of the cube (2^3=8 corners) and the center point run the center of the cube. These trials make up a portion of the Optimization design known as the "face centered central composite."[3] This design consists of the factorial experiments, center point run, and trials at the middle of each face (thus face centered) of the cube. In this way, runs are made at three levels of each variable to allow for determination of nonlinear terms in the model equation.

2.2 Experimental Results

The critical variables for the ECR etching of GaAs were known from previous studies, therefore screening was not required for this investigation.[4] It was not known, however, if the etch rate would be a linear or nonlinear function of the variables.

Therefore, a Discovery design and analysis was a good starting point, even though measured data, then Optimization experiments would not be needed. It was found that a nonlinear relationship did exist, so Optimization was required to model the etch rate.

As mentioned previously, a full factorial design was selected for the Discovery experiments. This required eight etch trials at two levels (a 'high' level and a 'low' level) of each variable with one additional trial at a middle level of each variable. The choice for the range of each variable is generally chosen according to any prior knowledge of the process, system constraints, or both. The level for the pressure was chosen based on knowledge of the process from previous studies and the microwave power and bias levels were selected with consideration for possible system damage. (The microwave power supply maximum output was 1000 watts and the RF power supply was capable of achieving -1000 volts of dc bias.) The low and high levels for each variable were: pressure, 1 and 5 millitorr; microwave power, 100 and 300 watts; bias, -75 and -150 volts. The eight factorial combinations of these variables can be represented as the corners of a cube as depicted in Figure 2-1. In the diagram, the "+" indicates the high level and the "-" indicates the low level.

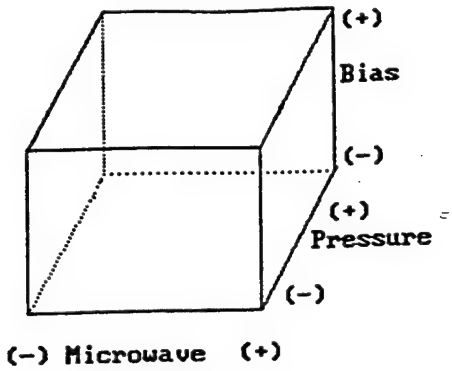

Figure 2-1. Representation of the experimental trials as a cube with each corner denoting a combination of the variables.

The "volume" enclosed by the cube therefore defines a "variable space", within which the final model equation (from Optimization) will attempt to predict (within a confidence interval) the etch rate for any level of the three variables. (The final equation is valid only for variable levels on or inside the cube.)

Table 2-1 gives the results of the full factorial Discovery experiments with center point run (#9). To measure the etch rate, a small dot of silver paint (for masking) was placed in the center of an approximately two cm^2 piece of GaAs and the sample etched for 30 minutes. After etching, the silver paint was removed with an acetone/methanol/distilled water rinse and the step height measured with a Dektak profilometer. Discovery analysis of the data revealed that the best model was obtained by performing a square root transformation of the response (taking the square root of the etch rate values in Table 2-1). Response transformations are commonly used in empirical modeling to more normally distribute the data.

Trial #	Pressure (Millitorr)	Mic. Power (Watts)	Bias (Volts)	Etch rate (Å/minute)
1	1	100	-75	93
2	1	300	-75	257
3	1	100	-150	221
4	1	300	-150	705
5	5	100	-75	0
6	5	300	-75	150
7	5	100	-150	238
8	5	300	-150	378
9	3	200	-112.5	371

Table 2-1. Results of the Discovery experiments.

For the Discovery experiments, the square root transformation improved the confidence levels of the model and the standard error of the predicted response.

Discovery (and Optimization) analysis of a designed set of experiments generates several confidence levels (from 0 to 100%) which indicate how well, or how confident one is, that the model represents the data. For the data in Table 2-1, the "percent confidence" in the model was 99.2%. This value, which should be large, gives the confidence that the model is real and doesn't simply represent experimental error. The "variation accounted for by the model" was 99.64% (which also should be large) and indicates the confidence that all critical variables have been included in the experiments.

The "coefficient of variation" was 6.04%. This value gives a measure of the size of the experimental error relative to the mean (predicted value at the center point) and should be small. The "standard error of estimate" was 0.862. This value should be small and ±2x(standard error of estimate) is the 95% confidence interval for the model predicted values. The final value, and one that is unique to Discovery, was the "percent confidence" in the nonlinearity observed at the center point. The measured etch rate at the center point was 371 Å/min. and the predicted value was 204 Å/min. which indicates that nonlinearity exists. The corresponding percent confidence that this was real (and not due to experimental error) was 97.2%. These results suggest that effects of experimental error were small and all the variables important to the response had been included. The design and analysis of experiments to resolve the nonlinear effects using Optimization is described next.

The Optimization design chosen was a "face centered central composite" which consists of the nine Discovery trials, trials at the center of each face of the cube (see Figure 2-1), plus two additional runs at the center point conditions.[3] The two replicated runs at the center point are used by Optimization analysis to estimate the experimental error in the developed model. The results of the eight runs (six faces plus two center points) are given in Table 2-2.

Optimization analysis of the complete set of experiments (Tables 2-1 and 2-2) found that the highest confidence levels for the model equation were obtained with no transformation of the response.

Trial #	Pressure (Millitorr)	Mic. Power (Watts)	Bias (Volts)	Etch rate (Å/minute)
10	3	100	-112.5	300
11	3	300	-112.5	416
12	3	200	-75	0
13	3	200	-150	477
14	1	200	-112.5	663
15	5	200	-112.5	302
16	3	200	-112.5	361
17	3	200	-112.5	378

Table 2-2. Results of the additional Optimization experiments.

A percent confidence for the terms in the model was also calculated (by Optimization) and it was found that all three of the linear terms (variable x coefficient), the two quadratic terms of bias and pressure (variable^2 x coefficient), and one interaction term of microwave x pressure (variable$_m$ x variable$_n$ x coefficient) had high confidence levels. By deleting the remainder of the terms, the percent confidence in the model and variation accounted for by the model were maximized while the standard error of estimate and coefficient of variation were minimized. These four values were:

Percent confidence in the model: 99.9%

Variation accounted for by the model: 86.8%

Standard error of estimate: 90 Å/minute

Coefficient of variation: 23.7%

The developed model equation was:

$$E = -1764 + 1.725M - 0.22MP + 32.8B - 0.13B^2 - 95.1P + 16.05P^2 \qquad (1)$$

where E is the etch rate, M is the microwave power in watts, P is the pressure in millitorr, and B is the rf induced dc bias in +volts. From equation (1), it can be seen that over the parameter range studied the effects of the microwave power and bias were positive and the effect of the pressure was negative. Therefore, an increase in the microwave power and bias voltage causes an increase in the etch rate while an increase in pressure causes a decrease in the etch rate. The measured and predicted etch rates for the 17 total trials are given in Table 2-3. The standard error of estimate of 90 Å/min. gives a 95% confidence interval of ±180 Å/min. This means that for any level of the process variables within the variable space, the probability that the measured etch rate will fall within ±180 Å/min. of the predicted value is 0.95. Looking at Table 2-3, runs 2, 3, 13, and 14 show a large difference between the measured and predicted response, exhibiting the rather substantial error bar in the predictability of the model. It is possible that this was due to experimental error, but unlikely. One possible reason for the large error bar could be that

Trial #	Measured (Å/min)	Predicted (Å/min)
1	93	50
2	257	350
3	221	354
4	705	654
5	0	-35
6	150	86
7	238	269
8	378	390
9	371	380
10	300	275
11	416	486
12	0	49
13	477	353
14	663	532
15	302	358
16	361	380
17	378	380

Table 2-3. Measured and model predicted etch rates.

the etch rate is a more complicated function of the process variables than that given by equation (1).

An additional Optimization capability is the response surface plot. For this investigation, the total response surface plot is "contained" within the "variable space" and is made up of smooth, 3-D surface contours. Each contour defines a surface of equal response magnitude and is continuous throughout the space, except at the edges, where they terminate. Optimization will generate a 2-D cross section of the 3-D plot in two of the variables with the third variable held constant. The third variable can be manually varied to create a collection of 2-D plots which can be visually inspected to give an idea of the shape of the 3-D, total response surface plot. The purpose of the response surface plot is to identify the optimum operating point for the process. The optimum (or

maximum) point for the etch rate was found to be at an operating pressure of 1 millitorr as shown in Figure 2-2. From the plot, the optimum levels for the microwave power and bias are 300 watts and -128 volts, respectively. It appears that the etch rate continues to increase as the microwave power is increased, but a peak is reached as the bias is increased. This may be interpreted (if the model is correct) as a leveling off of the sputter component (Ar) of the etch with possibly a decrease in the chemical component of the etch as the bias is increased past ~ -128 volts. It is also possible that the model is incorrect in this region of the variable space, however no trials were performed in this region.

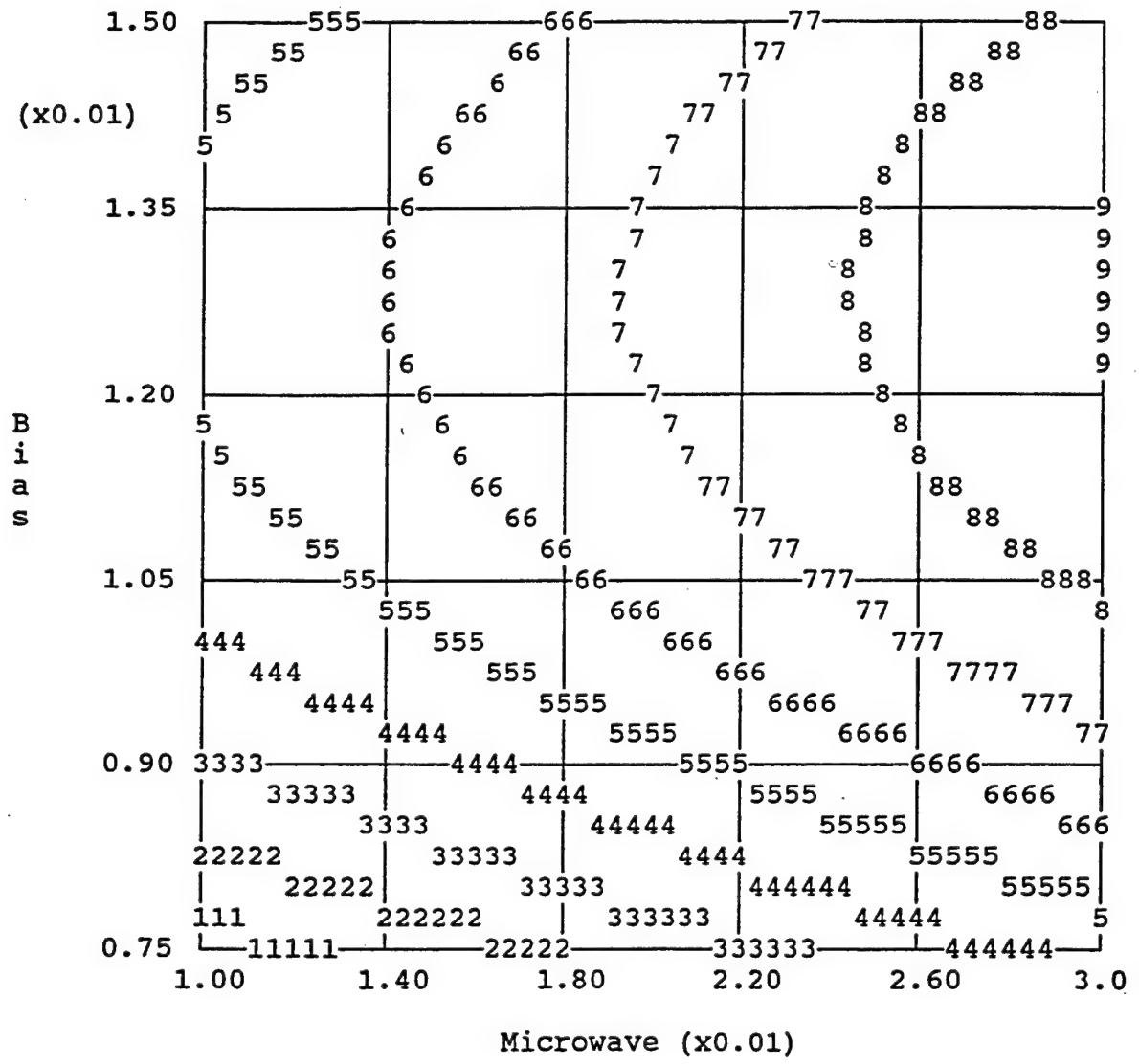

Figure 2-2. Response surface plot of the predicted etch rate at 1 millitorr pressure. Contours are in Å/min. with 1=79, 2=158, 3=237, 4=316, 5=395, 6=474, 7=553, 8=632, 9=711.

3. Etch Induced Surface Damage in GaAs and AlGaAs

In-situ ellipsometric measurements were taken on separate bulk GaAs samples during the etching studies performed in Chapter 2. The psi (ψ) and delta (Δ) data from the etched samples differed significantly from unetched samples, indicating that at least the near surface region had been altered by the etch. Damage created by ECR etching with a $CH_4/Ar/H_2$ plasma has been reported[9], but the exact cause and type of the damage has not been identified. To determine the characteristics of the damage, bulk GaAs was etched in the $CH_4/Ar/H_2$ mix, a pure hydrogen, and a pure argon plasma and the samples analyzed using *ex-situ*, variable angle of incidence spectroscopic ellipsometry (VASE) and Auger Electron Spectroscopy (AES). Using the results of these experiments and a partially etched, half micron thick AlGaAs film on a GaAs substrate, *ex-situ* VASE was also used to characterize the etch induced damage in AlGaAs. Prior to discussing the damage, an overview of ellipsometry will be presented.

3.1 Ellipsometry Overview

Ellipsometry is an optical technique that measures the change in polarization state of a linearly polarized light beam after reflection from (or transmission through) a sample.[10] The incident, linearly polarized beam becomes (in general) elliptically polarized after reflection due to the difference between the complex Fresnel reflection coefficients parallel (r_p) and perpendicular (r_s) to the plane of incidence. (The plane of incidence is defined as the plane containing the incident and reflected beams.) A diagram of this situation is given in Figure 3-1. The incident (linearly polarized) beam can be decomposed into electric field vectors oscillating parallel (**p**) and perpendicular (**s**) to the plane of incidence. An optical beam is linearly polarized when the **p** and **s**

polarization are oscillating in phase. In the elliptically polarized state, the **p** and **s** components are oscillating out of phase, and at a fixed plane in space (the plane perpendicular to the wave vector), the tip of the resultant electric field vector traces out an ellipse.

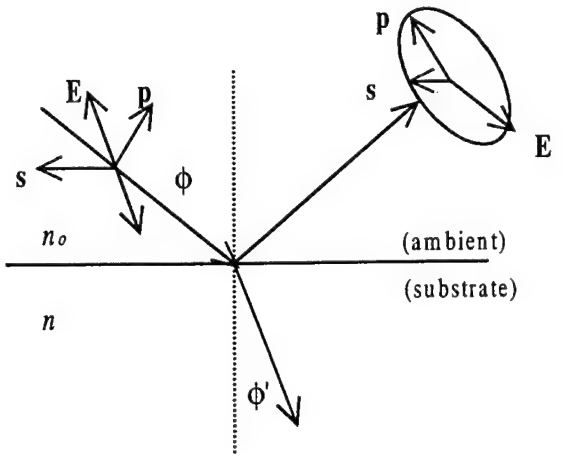

Figure 3-1. Change in polarization state of an optical beam after reflection from a bare substrate.

For the situation in Figure 3-1, the (complex) Fresnel reflection coefficients are:

$$r_p = \frac{n\cos\phi - n_o\cos\phi'}{n\cos\phi + n_o\cos\phi'} \qquad (2)$$

$$r_s = \frac{n_o\cos\phi - n\cos\phi'}{n_o\cos\phi + n\cos\phi'} \qquad (3)$$

and the ratio r_p/r_s can be written as:

$$r_p/r_s = \tan\psi e^{j\Delta} = \rho \qquad (4)$$

where tanψ is the amplitude ratio ($|r_p|/|r_s|$) and Δ is the phase difference (Δ_{rp}-Δ_{rs}). Ellipsometry measures the values ψ and Δ. For the simple case in Figure 3-1 of an ambient/substrate system, the complex index of refraction n can be found, after a little algebra, to be

$$n = n_o \tan\phi[1 - 4\rho(1 - \rho)^{-2}\sin\phi]^{1/2} \qquad (5)$$

and the pseudodielectric function ($<\varepsilon>$) is given by

$$<\varepsilon> = <\varepsilon_1> + i<\varepsilon_2> = \sin^2\phi[1 + \tan^2\phi(1 - \rho)^2/(1 + \rho)^2]. \qquad (6)$$

For the case of an ambient/film/substrate system as in Figure 3-2, the total reflection coefficients for the **p** and **s** polarization can be written as:

$$R_p = \frac{r_{01p} + r_{12p}e^{-j2\beta}}{1 + r_{01p}r_{12p}e^{-j2\beta}} \qquad (7)$$

$$R_s = \frac{r_{01s} + r_{12s}e^{-j2\beta}}{1 + r_{01s}r_{12s}e^{-j2\beta}} \qquad (8)$$

where $\beta = 2\pi n_1(d/\lambda)\cos\phi_1$ and ϕ_1 can be calculated from Snell's law.[10] Calculation of R_p and R_s for multilayered samples yields additional terms, but the form of the expressions remain similar. Equation (4) can then be rewritten as:

$$\rho = R_p/R_s = \tan\psi e^{j\Delta}. \qquad (9)$$

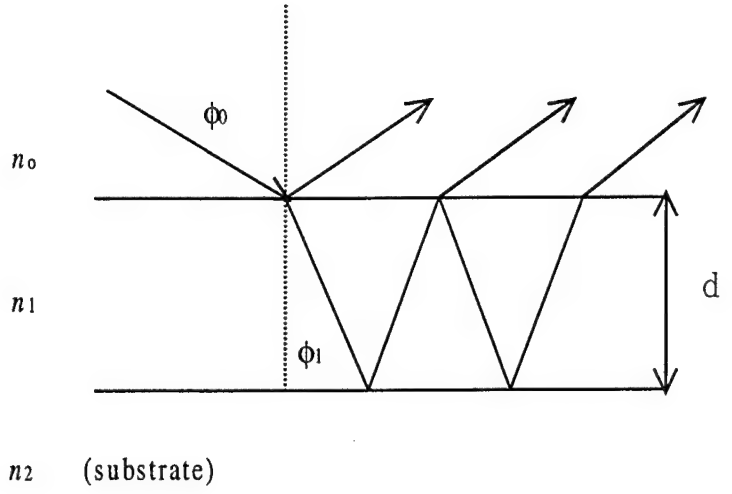

Figure 3-2. Reflection of a light beam from a (single) filmed substrate.

If the angle of incidence ϕ_0, indices of refraction n_0, n_1, n_2, and wavelength λ are known, then regression analysis can be used to solve for 'd' by finding the "best fit" between the measured ψ and Δ and the ψ and Δ calculated from a model of the material system. The best fit is found by varying 'd' (and perhaps other parameters) in the model until the Mean Square Error (MSE) is minimized. For the regression algorithm used in the W.V.A.S.E.™[5] software, the MSE is given by[11]:

$$\text{MSE} = \left[{}_{1/(N-M)} \sum_i \left(\left[(\psi_{cali} - \psi_{expi})/\sigma_{i\psi} \right]^2 + \left[(\Delta_{cali} - \Delta_{expi})/\sigma_{i\Delta} \right]^2 \right) \right]^{1/2} \qquad (10)$$

where 'N' is twice the number of wavelengths (88), 'M' is the number of fit parameters, 'σ' is the calculated standard deviation of the measurement, and '*i*' denotes the summation over all wavelengths (44).

Ellipsometry is sensitive to material parameters such as microstructure, alloy fraction, void fraction, and surface roughness. An accurate model must account for these properties, therefore parameters other than the thickness must be allowed to vary in the model. Solving for several parameters simultaneously can result in correlation between the variables, so care must be taken when working with complex material systems. As a general rule, a simple model should be used initially and then more parameters varied until parameters become correlated and/or no new information can be obtained.

There are many different ellipsometer configurations such as the null, phase modulated, and intensity modulated ellipsometers.[10] The M-44 used in this work was a Rotating Analyzer Ellipsometer (RAE), intensity modulated type which measures at 44 wavelengths simultaneously.[12] The M-44 system consists of a white light source (xenon lamp), collimator, prism polarizer, sample, rotating analyzer (second polarizer), dispersing optics (diffraction grating), and a photodiode array. After reflection from the sample, the light beam passes through the rotating analyzer where the intensity is modulated as the transmission axis of this second polarizer rotates about the polarization ellipse. The modulated beam then reflects off of the diffraction grating and onto the 44 element photodiode array. The sinusoidally varying intensity at each photodiode is then Fourier analyzed to calculate ρ.[12]

3.2 Damage Characterization

In-situ ellipsometry measurements of $CH_4/Ar/H_2$ ECR etched bulk GaAs are given in Figure 3-3. The E_1 and $E_1 + \Delta_1$ critical point features show a red shifting (shifting toward a lower energy) and broadening (spreading out in energy). The E_1 critical point feature is visible as a peak (at 2.9 eV) in $\langle\varepsilon_2\rangle$, the imaginary part of the pseudodielectric function, as given by the solid line in Figure 3-3. Included in Figure 3-3 are *in-situ* measurements at four and 48 seconds into a $CH_4/Ar/H_2$ etch at a pressure of 1 millitorr, 300 watts of microwave power, and -150 volts bias. The unetched spectrum (0s) was modeled (using the optical constants for GaAs obtained at UNL[13]) as a GaAs substrate with an approximately 60 Å thick overlayer of GaAs oxide. (It is unlikely that the native oxide on the sample was 60 Å, but more likely that the overlayer was a combination of oxide and residue left behind from the acetone/methanol/distilled water cleaning rinse.) The onset of the damage began almost immediately after the start of the etch and had stabilized by one minute. To investigate the cause of the damage, bulk GaAs was etched in pure H_2 and Ar plasmas (no etch can be obtained from a pure CH_4 plasma) and the samples analyzed using *ex-situ* ellipsometry. Figure 3-4 gives the second derivative of $\langle\varepsilon_2\rangle$ versus photon energy for unetched, $CH_4/Ar/H_2$, pure H_2, and pure Ar etched samples. The etch conditions for the H_2 were 0.5 millitorr, 300 watts microwave power, -100 volts bias and 1 millitorr, 200 watts microwave power, and -100 volts bias for the Ar etch. The H_2 etch resulted in the most severe red shifting and broadening while the Ar etch caused little red shift and very little, if any, broadening.

The approximate thickness of the damage layer for $CH_4/Ar/H_2$ and H_2 etched GaAs was determined empirically by etching these samples in an Ar plasma at the conditions given above. The measured etch rate for these conditions was determined by

the same procedure described in Chapter 2, and was found to be 330 Å/min. The *in-situ* $<\varepsilon_2>$ data at various times from an Ar etch of a previously etched sample ($CH_4/Ar/H_2$) is given in Figure 3-5. The E_1 peak (~2.8 eV at 0s) shifts back to approximately 2.9 eV (the value for "undamaged" GaAs) and has stabilized by 60 seconds into the etch. This implies that the damage layer for this sample was at most ~330 Å (1 min. x 330 Å/min. = 330 Å). *In-situ* measurements made on a sample which had been previously etched in H_2 showed that the Ar etch (same conditions as above) took considerably longer to shift the E_1 peak back to its "undamaged" value, indicating that the H_2 etch produced a much thicker damage layer. These results and the $<\varepsilon_2>$ measurements in Figure 3-4 suggest that the hydrogen in the $CH_4/Ar/H_2$ mixture is responsible for the red shifted damage layer.

Temperature and strain are two known causes of critical point energy shifting in crystalline GaAs.[14,15,16,17] However, the red shifting associated with a temperature increase is reversible, i.e. the critical point feature shifts back when the material is cooled to its original temperature. The results in Figure 3-4 show an irreversible red shifting, therefore a temperature effect cannot be the cause. Auger Electron Spectroscopy (AES) performed on unetched and H_2 only etched samples showed a Ga rich surface for the H_2 etch, as shown in Figure 3-6. This led to the hypothesis that the H_2^+ (or H^+) ions present in the plasma penetrate the surface and preferentially remove the As (reported as arsine, AsH_3)[9] from the lattice. The As depleted surface region expands slightly, resulting in a strained layer and corresponding red shifting of the E_1 feature. The increased removal of the As relative to the Ga would result in damage to the near surface crystal structure, which would account for the observed broadening.

An $Al_xGa_{1-x}As$ (x=0.28) heterostructure (AlGaAs on GaAs) also showed red shifting and broadening of the AlGaAs E_1 critical point feature after etching in a $CH_4/Ar/H_2$ plasma. Figure 3-7 gives a sequence of *in-situ* $\langle\varepsilon_1\rangle$ (real part of the pseudodielectric function) data measured at various instants during the etch. The etch conditions were 1 millitorr pressure, 300 watts microwave power, and -200 volts bias. The thickness of the AlGaAs layer was much greater than the penetration depth at E_1, therefore only the AlGaAs E_1 feature is visible, and not the GaAs E_1 feature. Also, the AlGaAs E_1 energy lies outside of the *in-situ* spectral range, so this feature is not seen for the "virgin" sample. (The "virgin" sample was best fit, or modeled, as a GaAs substrate with 5070 Å of $Al_{0.28}Ga_{0.72}As$[18] and 16 Å of GaAs oxide.) Immediately after the start of the etch, E_1 red shifts into the *in-situ* spectral range and becomes broadened. After ~60 seconds into the etch, the red shifting has stabilized, signifying that the damage layer has reached an equilibrium thickness. The change in $\langle\varepsilon_1\rangle$ below the band gap (~1.85 eV) is due to the removal of the AlGaAs layer. The light penetration depth is much greater below the gap and is more sensitive to the properties of the undamaged AlGaAs layer. The "hill" centered at ~1.75 eV is known as an "interference oscillation." These oscillations become damped at energies above the band gap due to the decreased penetration (absorption) at the higher photon energies.

After etching approximately half way through the AlGaAs layer, the sample was removed from the chamber and analyzed using *ex-situ* ellipsometry. The data was best fit with 2541 Å of AlGaAs and 57 Å of GaAs oxide as shown in Figure 3-8. The model fit well at the lower photon energies but became very poor at the higher energies, which are more sensitive to the near surface region. Profilometer measurements of an AlGaAs

heterostructure etched at the same conditions and for the same amount of time agreed very well with the thickness solution found above. Sequential fitting of the *in-situ* data (simulation of real time fitting) for a completely etched away AlGaAs sample using the model above (GaAs oxide for the overlayer), accurately tracked the removal of the AlGaAs down to ~2000 Å, at which point the fits became very poor. It was found that optically modeling the damage layer improved the "tracking range" of the ellipsometer down to ~900 Å of AlGaAs where other problems (to be discussed in Chapter 4) caused the fits to become unreliable. The optical modeling of the damage for GaAs and AlGaAs is described in the following section.

3.3 Optical Modeling of the Damage

The damage in GaAs was modeled (from a sample etched in the $CH_4/Ar/H_2$ mix) using *in-situ* data at one minute into the etch. The optical constants of the damage were obtained using the harmonic oscillator (HO) model[19] and assuming the sample consisted of a single layer of damaged material on a bulk (undamaged) GaAs substrate. The seven oscillator model[20] for crystalline GaAs was used initially to fit the data. Each oscillator has three variable parameters: the amplitude, broadening, and energy. A good fit was obtained by varying all three parameters for the E_1 oscillator, the amplitude for a higher energy oscillator, and the thickness of the damage layer. The thickness of the damage layer solved for using this model was approximately 150 Å. The damage thickness found from the Ar etching was ≤ ~330 Å, in fair agreement with the ellipsometrically determined value.

An identical approach was used to solve for the thickness and optical constants of the AlGaAs red shifted layer. The optical constants 'n' (index of refraction) and 'k'

(extinction coefficient) are given in Figure 3-9. The damage thickness solved to about 120 Å for AlGaAs, slightly less than that found for GaAs.

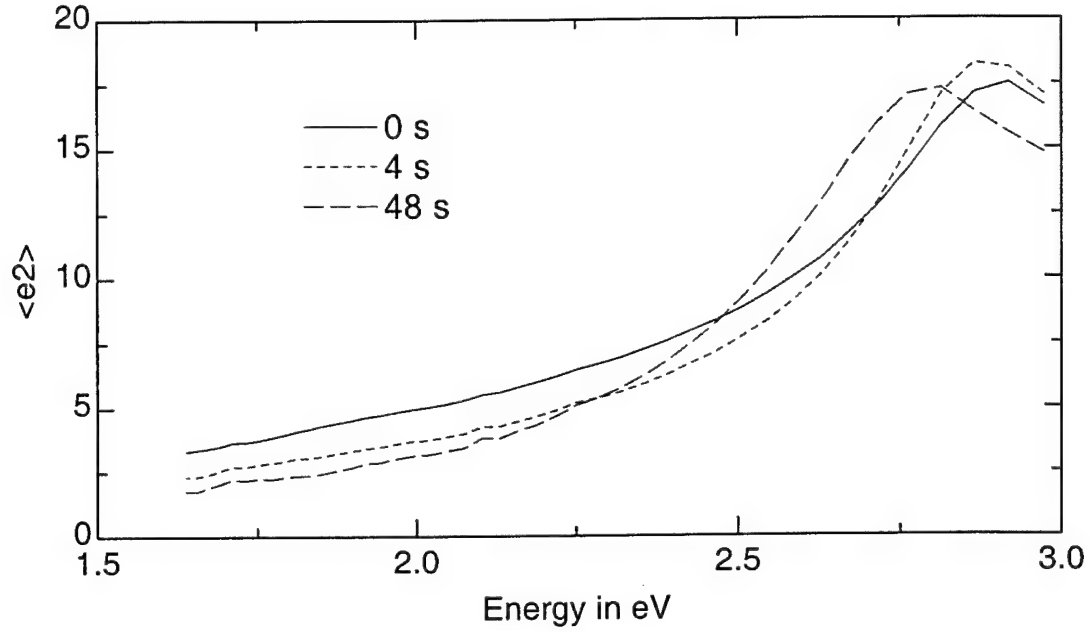

Figure 3-3. *In-situ* pseudodielectric function (imaginary part) measured during $CH_4/Ar/H_2$ etching of GaAs.

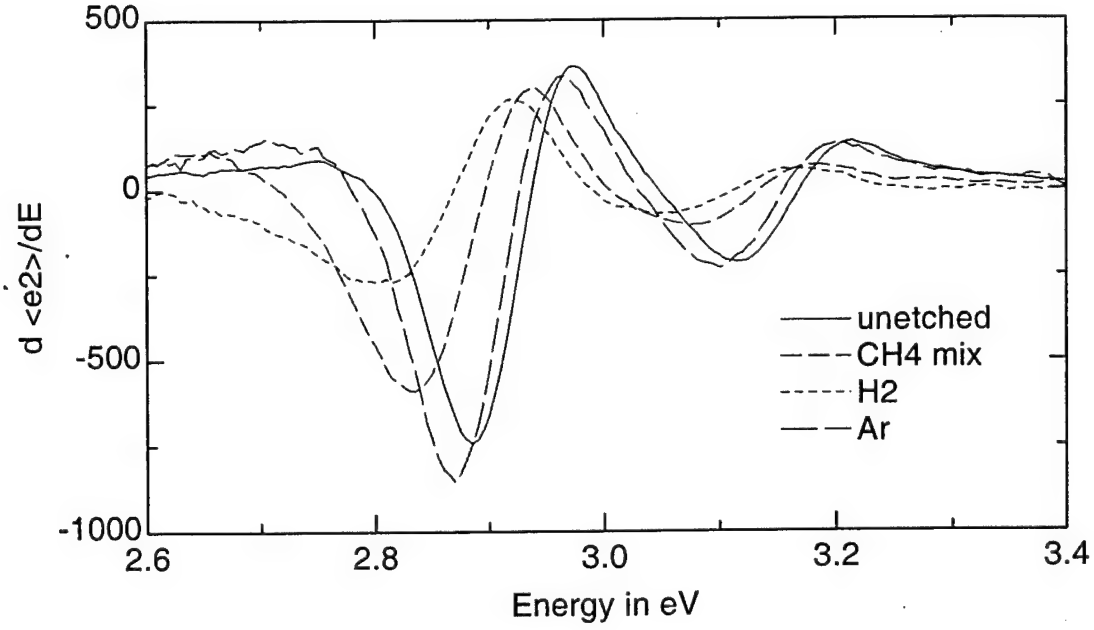

Figure 3-4. Second derivatives of *ex-situ* $<\varepsilon_2>$ measured for unetched, CH_4 mix, H_2, and Ar etched GaAs.

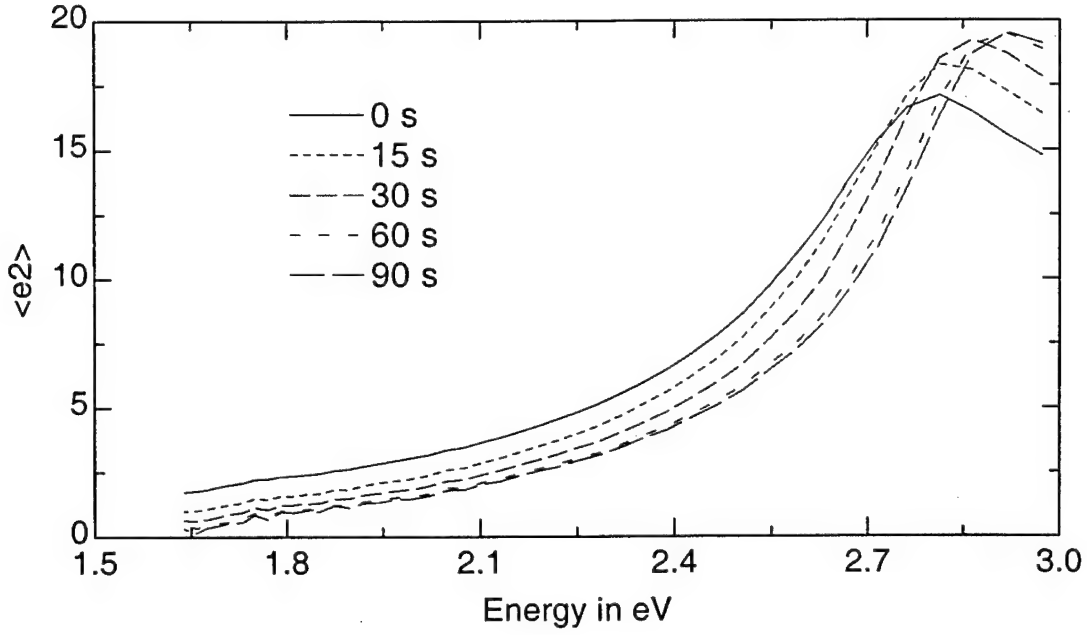

Figure 3-5. *In-situ* $<\varepsilon_2>$ measured during Ar etching of GaAs that was previously etched with $CH_4/Ar/H_2$.

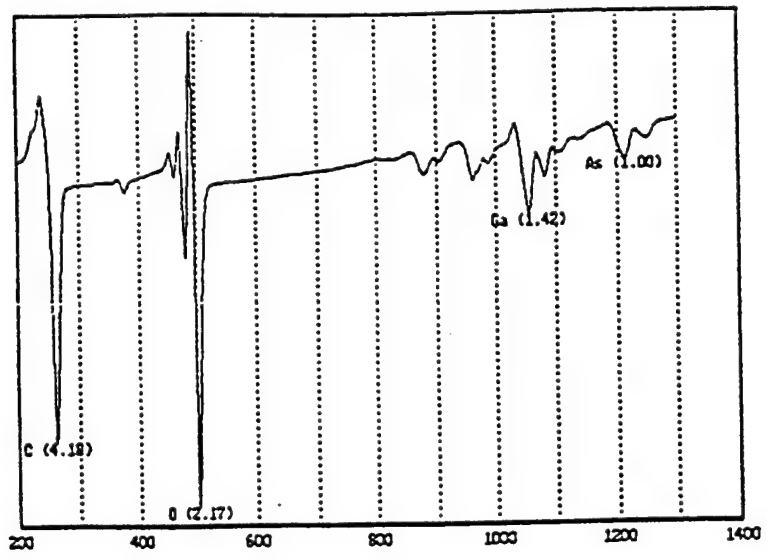

Figure 3-6 AES plot of dN/dE vs electron energy for virgin GaAs.

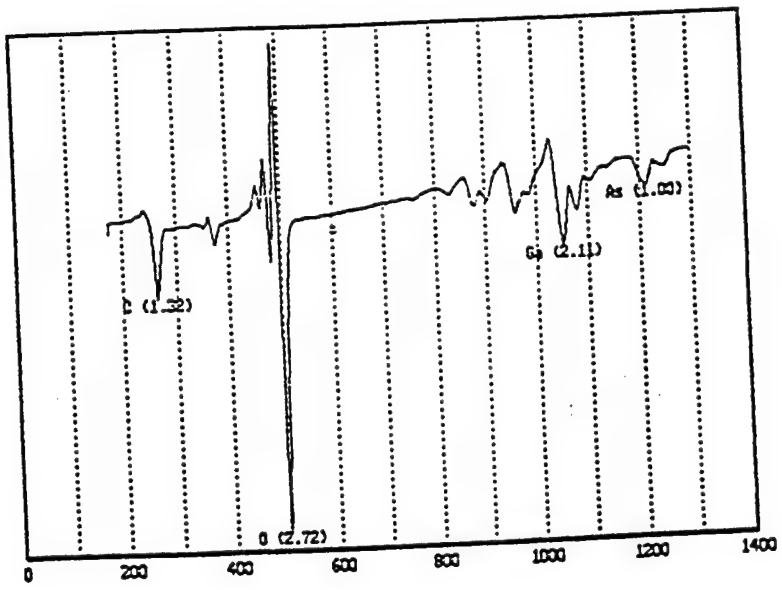

Figure 3-6 (continued) AES plot of dN/dE vs electron energy (eV) for H_2 etched GaAs.

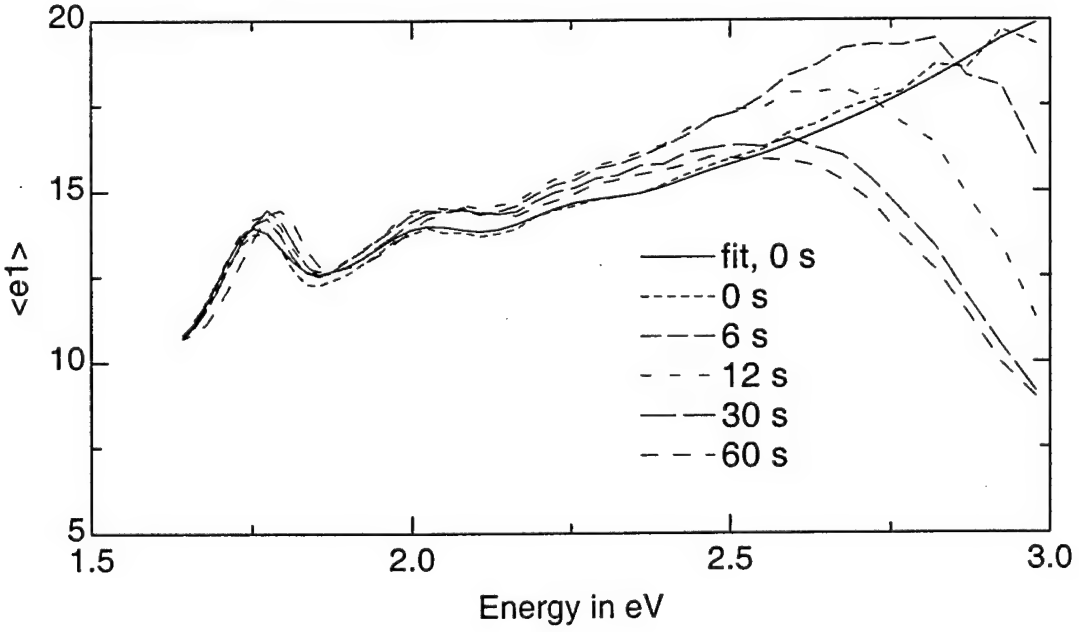

Figure 3-7. Real part of the pseudodielectric function measured during $CH_4/Ar/H_2$ etching of an AlGaAs/GaAs heterostructure.

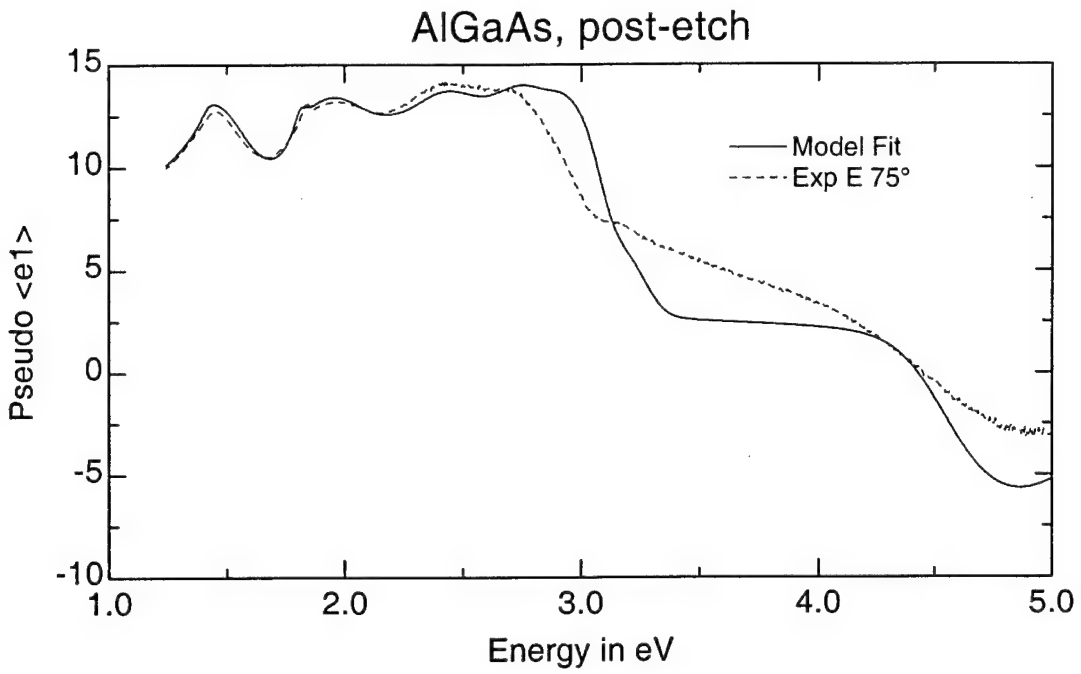

Figure 3-8. Ex-situ measured real part of the pseudodielectric function and model fit for $CH_4/Ar/H_2$ etched AlGaAs using a GaAs oxide overlayer.

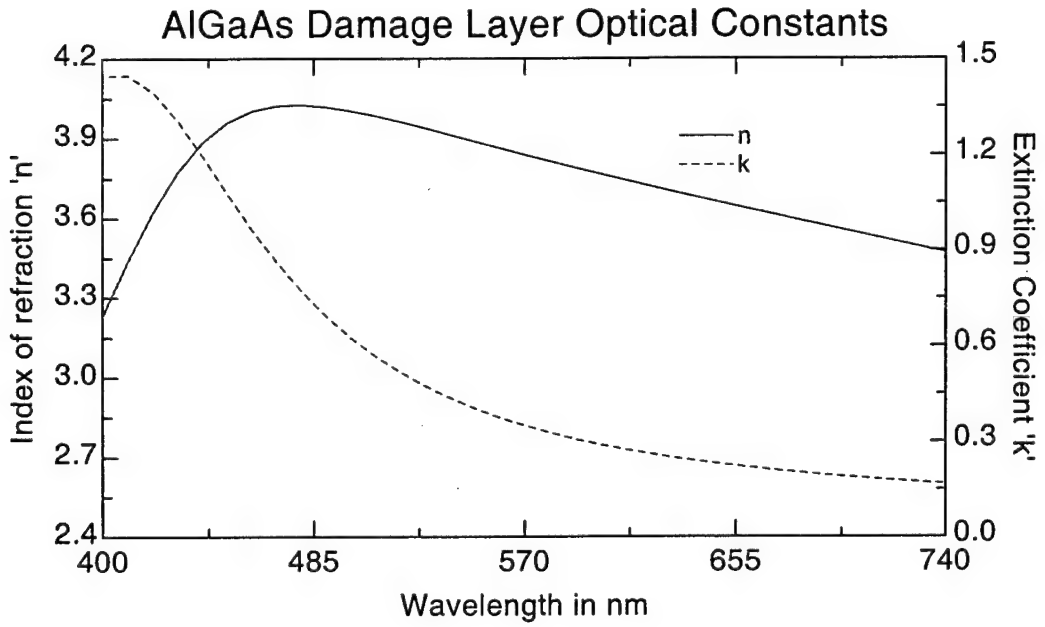

Figure 3-9. Damage layer optical constants for $CH_4/Ar/H_2$ etched AlGaAs.

4. Etch Control

The desire for smaller and faster semiconductor devices requires tighter control of the process steps used in integrated circuit (IC) fabrication. Etching of semiconductors and photoresist materials are important processes for which ellipsometry is well suited as a diagnostic tool. Ellipsometry is unaffected by the plasma environment and can provide accurate real time information about material parameters such as film thickness, composition, and uniformity. Combined with the computational power of a personal computer (PC), state-of-the-art ellipsometry can acquire data and solve for film thickness in less than a second.

One of the tasks of an *in-situ* etch process monitor is the detection of the etch end point. *In-situ* ellipsometry can lose accuracy at very thin film thickness for some material systems, therefore end point detection cannot be accomplished directly from ellipsometer measurements in some applications. However, the end point can be determined (for these applications) from an accurate etch rate calculation and known thickness before the film becomes "critically" thin. For example, if it is desired to etch a film down to a thickness d_1 (d_1 possibly zero), and at a thickness d_2 an accurate etch rate (R_e) is calculated, then the time required to etch to d_1 and stop, is given by $(d_2 - d_1)/R_e$. An etch rate can also be used to calculate a percent over-etch time, which is commonly used in IC fabrication.

The M-44 operating software W.V.A.S.E.™[5] was integrated with a control algorithm through an External Programming Interface (EPI) to function as an end point detection system. Through the EPI, commands could be passed to W.V.A.S.E.™[5] from the control program and layer thickness and elapsed time data (and any other selected fit

parameters) could be passed from W.V.A.S.E.™[5] to the control. The control, in turn, was directly or indirectly interfaced with the microwave and rf power supplies to adjust or terminate the etch. The microwave power supply was actively adjusted from the control program via the ellipsometer control module (EC-100). The rf power supply was similarly controlled, except through an RS-232 serial port on the PC. The ellipsometer/PC system therefore served as a feedback loop to control the etch process. This chapter describes the implementation and results of the work done to use the M-44 SE as a means to control the etching of III-V semiconductors (AlGaAs/GaAs heterostructure) and photoresist materials.

4.1 Control Implementation

The M-44 was computer controlled via the W.V.A.S.E.™[5] software running in a Windows™ environment on an IBM compatible, 486 DX2, operating at 33 Mhz. The control algorithm was written in Microsoft Visual Basic (VB) and also runs in the Windows™ environment. The link established between W.V.A.S.E.™[5] and the VB control (VBC) was initiated and defined within the VBC program. The type of link used for this application was a "hot link" whereby W.V.A.S.E.™[5] automatically passes selected fit parameters, the elapsed time of the etch (W.V.A.S.E.™[5] data acquisition was started simultaneously with the etch), and the MSE. The data gets passed to an object in the VBC called a "text box." The changing of the contents in this box invokes an "event procedure" (the change in contents is the "event") which consists of the lines of code associated with the object. When an object experiences an event (an event can be a mouse click, double click, etc.), the code contained within that object's "event procedure" is executed. This type of program flow is known as event driven execution.

If no code is executing, the VB application is in a "stand by" mode, waiting for an event to occur.

The VBC was written using a single "form" or window. Contained within the window are all of the objects (command buttons and text boxes) needed to display important information and manipulate W.V.A.S.E.™[5] and the microwave and rf power supplies. A picture of the window is given in Figure 4-1.

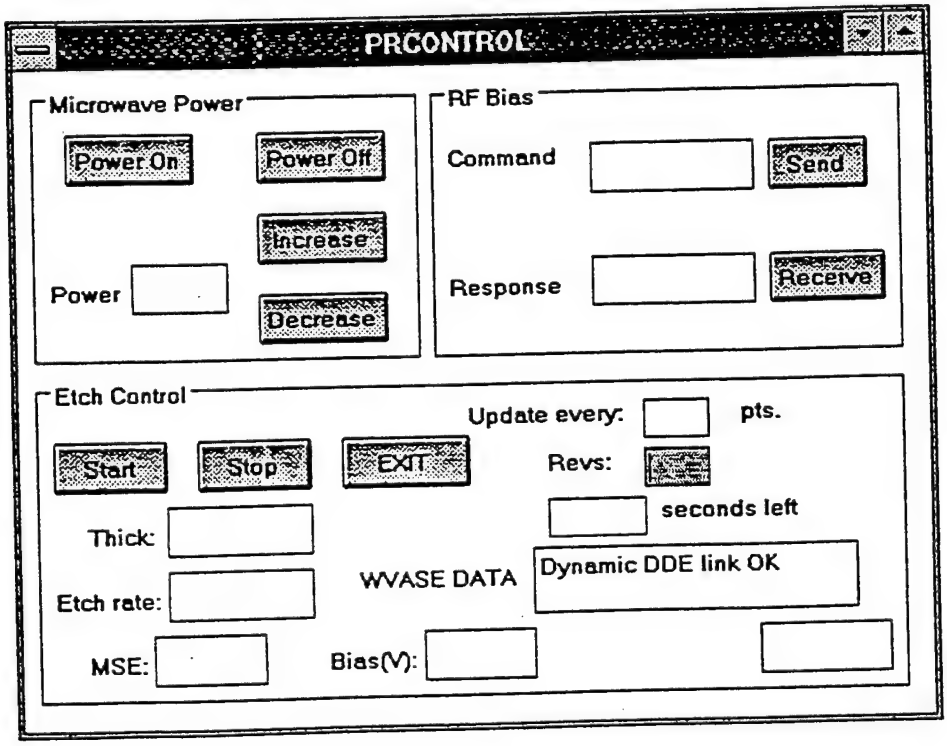

Figure 4-1. Picture of the VBC window.

The command buttons and text boxes in the upper two captioned frames were used to control the microwave and rf power supplies. These two sections were primarily needed to establish the initial etching conditions. The lower frame contains the objects

for starting and stopping the etch, receiving the W.V.A.S.E.™[5] data (text box labeled "WVASE DATA"), and displaying the current thickness, etch rate, MSE, and bias voltage. (The "update every" and "Revs" text boxes were used for graphing purposes.)

The complete procedure for using the system for etch control is as follows. First, the sample is loaded into the chamber and the pump down is started. After the system reaches a base pressure of typically 7×10^{-7} Torr, the sample is translated such that the ellipsometer probe beam is approximately centered on the sample. The ellipsometer is then aligned and a calibration performed.[20] The calibration gives ψ and Δ data for the sample which is used to fit for the model parameters and the angle of incidence. (The angle of incidence is fixed at this value during the etch run.) The necessary fit parameters (typically 1 or 2 layer thickness and occasionally thickness nonuniformity) are then selected while in W.V.A.S.E.™[5], or the appropriate commands are sent to W.V.A.S.E.™[5] from the VBC. The next step is to place a shutter in front of the sample and establish the plasma. The control is then started and the shutter removed simultaneously.

The ellipsometer then begins taking measurements (at a user specified frequency) and passing the fit parameter solutions to the VBC. The layer thickness values and elapsed time are stored in an array for etch rate calculations. After a specified number, 'D', of data points are stored (each thickness and corresponding time are considered one data point), the VBC calculates an etch rate by fitting a straight line to the 'D' data points. Once the etch rate calculations begin, the "main" procedure in the VBC (that invoked by the change in the "WVASE DATA" text box) tests the incoming data and performs the necessary functions according to the programmed etch scheme. Various

schemes were attempted and will be discussed in detail in the following sections on photoresist etching (4.2) and AlGaAs/GaAs heterostructure etching (4.3).

4.2 Photoresist Etching

The photoresist (PR) samples were used as an inexpensive means to test and debug the VBC for AlGaAs/GaAs etching. These samples were single and double layers of PMGI and 1400-27 type PR materials on silicon and were cut from 10 cm diameter wafers. (PMGI and 1400-27 are the brand names of the PR manufacturers.) These wafers were provided by the Air Force to compare the etch rates of each material in oxygen and N_2O ECR plasmas. The etch rates were determined ellipsometrically by *in-situ* monitoring of the etching of the single layer samples. The M-44 was capable of accurately determining the film thickness of these samples during the etch. It was also possible to ellipsometrically determine the thickness of the active layer (layer being etched) during etching of the two layer 1400-27/PMGI/Si sample as the 1400-27 was completely removed and the PMGI layer began to etch.

The optical constants ('n' and 'k') and layer thickness of each of the PR samples were unknown prior to conducting the O_2 and N_2O etch rate comparisons. In order to ellipsometrically model the samples, these parameters were needed. This work was done by Professor Paul Snyder at UNL using *ex-situ* VASE. The PMGI and 1400-27 single layer samples were both modeled using an isotropic Cauchy formula[21], where 'n' and 'k' are given by:

$$n = A_n + B_n/\lambda^2 + C_n/\lambda^4 \qquad (11)$$

$$k = A_k \exp[-B_k(12400/\lambda - 12400/C_k)] \qquad (12)$$

where A_i, B_i, C_i are constants and λ is the wavelength in angstroms. The optical constants found using the Cauchy model for the PMGI sample are given in Figure 4-2. Using these optical constants, the measured pseudo $<\varepsilon_1>$ and $<\varepsilon_2>$ were fit by varying the layer thickness. Measured and generated pseudo $<\varepsilon_1>$ and $<\varepsilon_2>$ are given in Figure 4-3. The thickness solved to 1070.7 nm for the PMGI layer. The optical constants found for the 1400-27 sample are given in Figure 4-4 and the $<\varepsilon_1>$ and $<\varepsilon_2>$ fits are given in Figure 4-5. The 1400-27 thickness solved to 1380.2 nm. Using the optical constants from the single layer samples, $<\varepsilon_1>$ and $<\varepsilon_2>$data from the 1400-27/PMGI/Si sample were fit by varying the thickness, as shown in Figure 4-6. The individual layer thickness solved to 1073.7 nm for the 1400-27 and 1380.6 nm for the PMGI. These values were very close to those found for the single layer samples, likely a result of each individual material being deposited on all samples in one step.

Testing of the system was done exclusively with the 1400-27/PMGI/Si samples. There were few problems associated with controlling the etch of the PR sample, but one problem (which seemed trivial at first) posed significant trouble. As remarked upon earlier, an over-etch is commonly used in wafer processing to assure that a layer is completely removed over the entire wafer surface. An over etch is typically calculated as a percentage of the original film thickness or as a percentage of the time required to "just" remove the layer. In either case, the over-etch is calculated as a time to continue etching, which requires the use of a timer to terminate the etch. Visual Basic provides a timer which generates a "timer event" once a preset amount of time has elapsed. The timer event causes VB to execute the code associated with the timer object. However, the timer event is very low in priority, which means that if VB or W.V.A.S.E.™[5] is

executing code at the instant the timer event is generated (which was always the case), the timer procedure will not be executed. Also, the VB timer could only count to 64 seconds, not much of an over-etch. This problem was overcome by storing the value of the system clock in a variable at the point when the over-etch period started, adding the over-etch time to this variable, then testing this variable against the system clock in the "main" procedure to terminate the etch. This method worked to within an accuracy of less than one second for the PR sample. (It was also possible to terminate data acquisition and use the timer in conjunction with a loop to stop the etch. The W.V.A.S.E.™[5] data is not used by the VBC after the over-etch time begins, therefore terminating data acquisition places the VBC in "stand by" mode, assuring that the timer procedure will be executed.)

An etch scheme employing bias reduction toward the end of the etch plus an over-etch was tested on the PR sample. Bias reduction was implemented to minimize the amount of etch induced surface damage left on the sample. This scheme was successfully applied as demonstrated in the following described control run.

The purpose here was to etch the top layer (1400-27) down to 70 nm, reduce the bias to -75V (from -100V), then over-etch for a time equivalent to 10% of the original 1400-27 thickness. The etch conditions were 300W microwave power, 2 millitorr pressure (O_2), and -100V (initial) of bias. The frequency of the ellipsometer measurements was set at one every 0.8 seconds and the number of data points ('D') needed to calculate an etch rate was set at three. After aligning and calibrating the ellipsometer, the model layer thickness and angle of incidence were solved. The 1400-27 and PMGI layers solved to 1390.7 nm and 1062.2 nm, respectively, and the angle of

incidence was solved to 74.3°. Thickness nonuniformity was also allowed to vary in the model and this value solved to 2.81%. Thickness nonuniformity was also fit for the samples used in the *ex-situ* VASE analysis, but solved to only ~1%. The spectral resolution of the *in-situ* ellipsometer (M-44) is much poorer than that of the *ex-situ* ellipsometer, which causes a "smearing out" of the interference oscillations (see Figures 4-3 and 4-4), and an apparent larger nonuniformity. (Thickness nonuniformity also causes a "smearing out" of the interference oscillations).

The fit parameters at the start of the etch were the 1400-27 thickness and nonuniformity. (It was discovered during testing that nonuniformity fitting was required or W.V.A.S.E.™[5] would lose track of the thickness shortly after the start of the etch.) Once the top layer was etched away, commands were sent from the VBC to delete the top layer in the model and start fitting for the PMGI layer thickness. Graphs of thickness and etch rate versus time of the etch are given in Figures 4-7 and 4-8, respectively. The portion of the thickness-time graph up to 6.5 minutes is the etching of the 1400-27 layer and the remainder is the PMGI removal. The bias reduction at 70 nm is clearly seen in Figure 4-8. Also in Figure 4-8, the etch rate is observed to increase significantly (to ~300 nm/min.) as the PMGI layer began to etch, a result found in the O_2/N_2O PR etch rate studies (the PMGI material etched much faster than the 1400-27 material).

The etch rate dropped from 215 nm/min. to 190 nm/min. after bias reduction, resulting in a VBC calculation of 45 seconds for an over etch time. The time measured by a stop watch was also 45 seconds. The last thickness obtained for the PMGI was 860 nm with 8.32% nonuniformity. A measurement with the *in-situ* ellipsometer after the etch found 820 nm of PMGI with 10.32% nonuniformity. The reason for the difference

was the deactivation of nonuniformity fitting when the model was changed at 0 nm of 1400-27. This property of W.V.A.S.E.™[5] was unexpected, but did not affect the results of the etch, as the objectives were met successfully.

A second scheme, used successfully on the PR only, was active etch rate control. It is advantageous to have a system automatically adjust to achieve a desired etch rate. In etching systems, performance degradation over time can lead to reduced etch rates and decreased throughput. If the process variables which increase the etch rate (Chapter 2) can be adjusted above their "nominal" values, the system can self adjust to maintain the "nominal" etch rate. When the system performance becomes so degraded that the expected etch rate is no longer achievable within system constraints, a diagnostic tool could be used to signal this situation.

To achieve etch rate control in the following described control run, a simple loop structure was incorporated into the VBC whereby a target etch rate (T_e) was compared to the calculated etch rate (C_e) and the bias adjusted proportionally to the difference, i.e., the larger the difference the larger the increase. An etch rate dependence for the 1400-27 material was estimated at ~1.5 nm/min. per volt of bias and the bias was adjusted according to the following: for $C_e \leq T_e$ - 20 nm/min. the bias was increased by -15V, and for T_e - 20 nm/min. $< C_e \leq T_e$ - 10 nm/min. the bias was increased by -10V. A final etch rate of $T_e \pm 10$ nm/min. was desired, with T_e chosen as 140 nm/min. Also, the VBC was configured to stop the etch at the interface between the 1400-27 and PMGI layers by tracking the 1400-27 thickness, and not by an etch rate projection.

The etch conditions for this run were 300W microwave power, 7 millitorr pressure (N_2O), and -70V (initial) of bias. The initial bias was selected because this

value was anticipated to give an etch rate significantly less than the target. Alignment and calibration were performed and the following model parameters were solved: 1400-27 thickness, 1152.3 nm (this layer had been previously etched slightly prior to this run, the original thickness was 1380 nm); PMGI thickness, 1056 nm; nonuniformity, 3.06%; and angle of incidence, 74.81°. The fit parameters during the etch were the top layer thickness and nonuniformity. The frequency of the ellipsometer measurements was set at one every two seconds and the number of data points needed to calculate an etch rate was 20. The resultant thickness-time and etch rate-time graphs are given in Figures 4-9 and 4-10, respectively.

At the initial bias setting of -70V, an etch rate of ~95 nm/min. was obtained, at which point the VBC increased the bias to -85 V. A corresponding slight increase in the slope of the thickness-time graph results, although this is difficult to see. Approximately one minute after the first bias increase, the calculated etch rate stabilizes at ~115 nm/min., where the bias is again increased by -15V to -100V. The etch rate then stabilizes at ~132 nm/min., within the desired ±10 nm/min. of the target rate (140 nm/min.). The etch continues at -100V bias until the interface is reached. The final thickness was 0 nm for the 1400-27 and 1050 nm for the PMGI, very near the interface. The final thickness nonuniformity solved to 4.8%, a consequence of the higher operating pressure (7 millitorr) relative to the previously described control run (2 millitorr and 8.32% nonuniformity).

4.3 AlGaAs/GaAs Heterostructure Etching

The control algorithms developed using the PR samples were applied to the etching of an AlGaAs/GaAs sample with limited success. The etch induced surface

damage and highly nonuniform etching of the ECR system made it difficult to ellipsometrically determine an accurate etch rate for end point projection. End point projection was needed with AlGaAs/GaAs because the *in-situ* (M-44) ellipsometer data became unreliable before the AlGaAs layer reached the desired thickness of 70 nm.

AlGaAs etching with the usual $CH_4/Ar/H_2$ flow ratios of 3.3/5/10 sccm and within the pressure ranges used in Chapter 2 produced large, but highly nonuniform etch rates over the probed sample area. The maximum etch rate measured was 51.8 nm/min. at 200W microwave power, -200V bias, and 3 millitorr pressure. To increase the etch uniformity, AlGaAs etch runs were attempted with the 3.3/5/10 flow ratios at seven millitorr. (Increasing the pressure homogenizes the active etching species in the plasma as they diffuse out of the ECR zone and impinge on the sample.) However, these trials resulted in a polymer deposition and no etching. Polymer deposition is indicative of an over abundance of CH_4 in the gas mix. It seemed that valving off the turbo pump to increase the operating pressure was changing the CH_4 to H_2 concentration ratio. As an educated guess, it was decided to lower the CH_4 flow rate and increase the Ar and H_2 flow rates. Etching with a $CH_4/Ar/H_2$ flow ratio of 2.5/6/25 sccm at 300W microwave power, -200V bias, and pressure of seven millitorr gave a much more uniform etch but at a significantly reduced rate of only 14 nm/min.

An AlGaAs/GaAs control run was conducted at the modified flow ratio given above. The etch scheme was to etch the AlGaAs layer to 200 nm, reduce the bias from -200V to -150V, and continue etching at -150V to 140 nm. Once the AlGaAs reached 140 nm, an etch rate calculation was used to project to an etch end point of 70 nm of AlGaAs. Before etching, the sample was best fit as a GaAs substrate, 504.3 nm of

$Al_{0.34}Ga_{0.66}As$, and 1.8 nm of surface GaAs oxide. The angle of incidence solved to 74.47°. The frequency of the ellipsometer measurements was set at one every six seconds and the number of data points needed to calculate an etch rate was 15. The model fit parameters for the etch were the AlGaAs layer and the damaged AlGaAs layer (the damage layer replaced the GaAs oxide for modeling during the etch). As there is no damage on the sample prior to the etch, the damaged AlGaAs layer was initially set to zero thickness.

The thickness-time graphs for the AlGaAs and damaged AlGaAs are given in Figures 4-11 and 4-12, respectively. Oscillatory fluctuations in the calculated AlGaAs thickness are clearly seen at four, 12, 18, and 26 minutes. The reason for these fluctuations is unknown, although it is possible that this was a real effect, perhaps due to a compositional non-homogeneity in the AlGaAs material. It is interesting to note that these "anomalies" occur at almost exactly equal spaced thickness of 450, 350, 250, and 150 nm. The bias reduction at 200 nm is also clearly seen as a change in slope in Figure 4-11. The graph terminates at 140 nm, where control was turned over to a timer and W.V.A.S.E.™[5] data acquisition was terminated. Damage layer formation began almost immediately after the start of the etch, reaching an equilibrium value of ~7 nm at two minutes. The damage layer thickness decreased after bias reduction, as expected. The ellipsometrically determined layer thickness after the etch were found to be 71 nm for the AlGaAs and 7 nm for the damaged AlGaAs. Thickness nonuniformity solved to 38%, but was not fit during the etch. Profilometer and WYCO interferometer measurements of the step heights on similarly etched (masked) samples showed good agreement with the ellipsometrically determined thickness nonuniformity. Identical etch

control runs done at the normal flow ratios and lower pressures resulted in thickness nonuniformity values ranging from 70-100%, which were also confirmed by profilometer measurements.

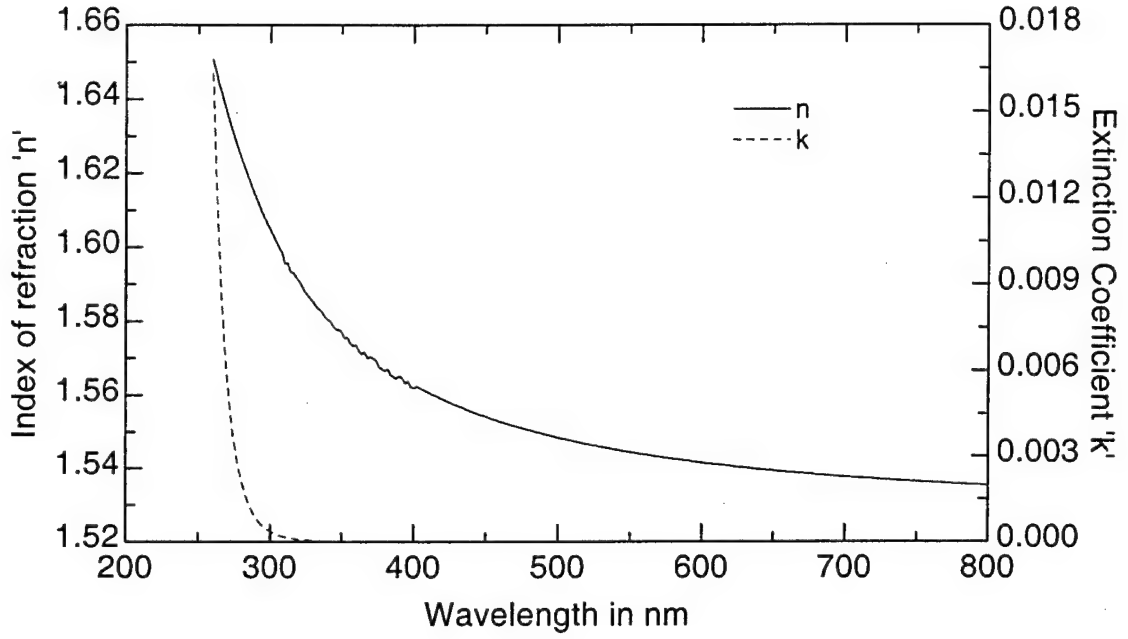

Figure 4-2. Optical constants for PMGI material.

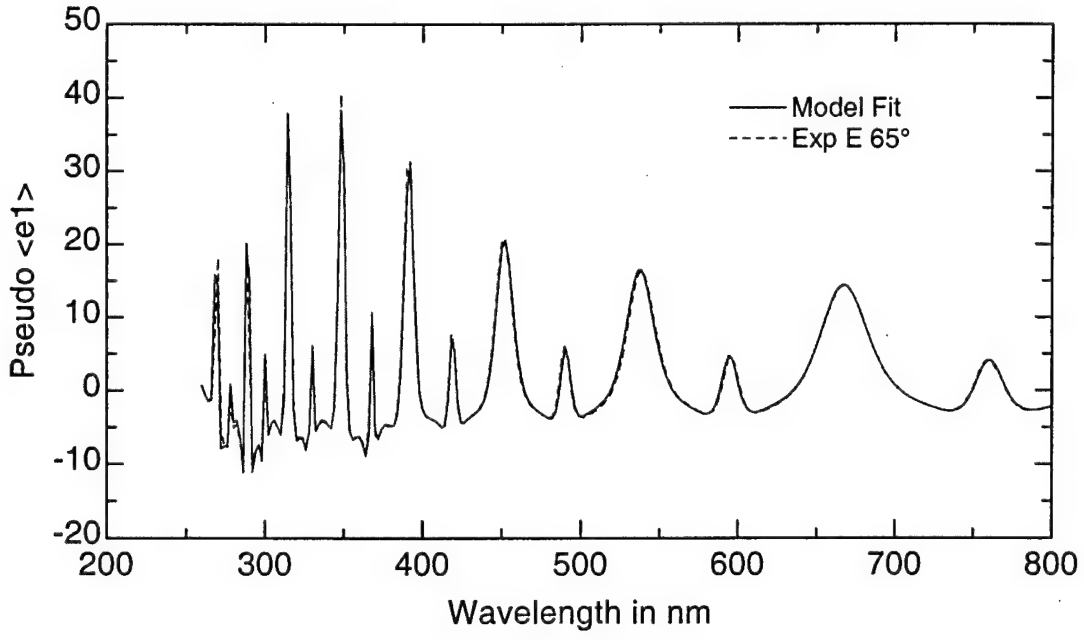

Figure 4-3. Fit to the PMGI sample.

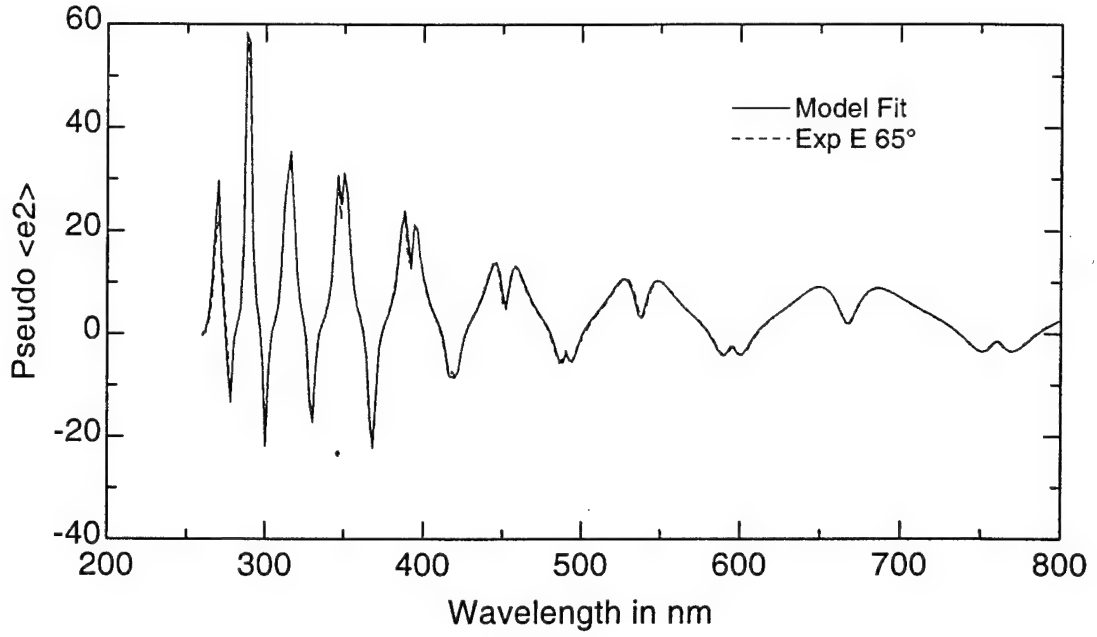

Figure 4-3. (continued)

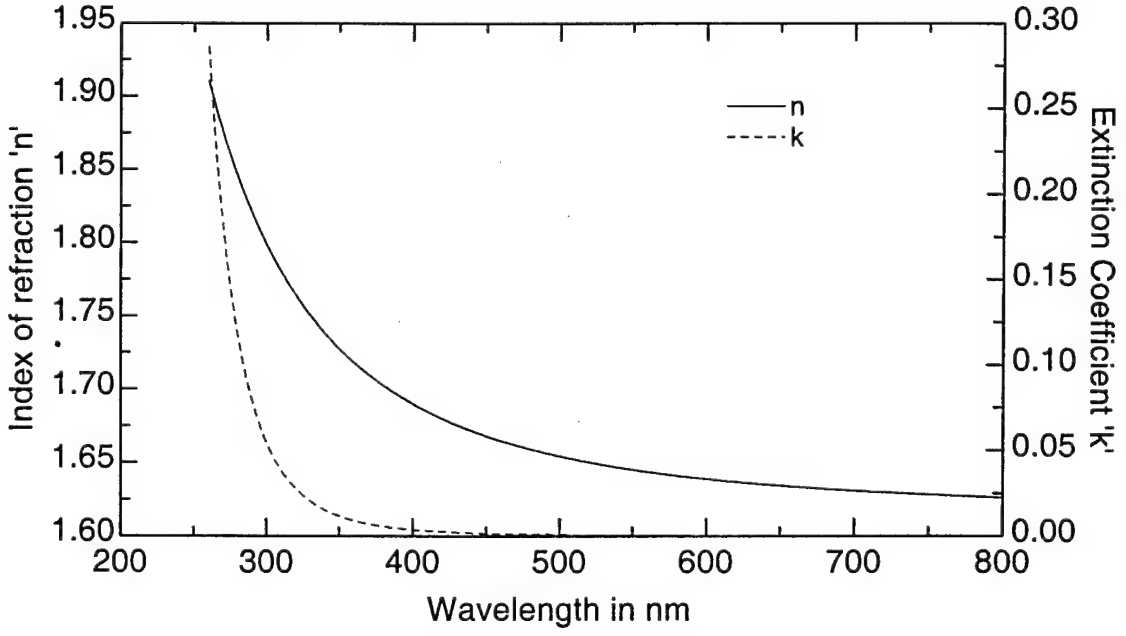

Figure 4-4. Optical constants for the 1400-27 material.

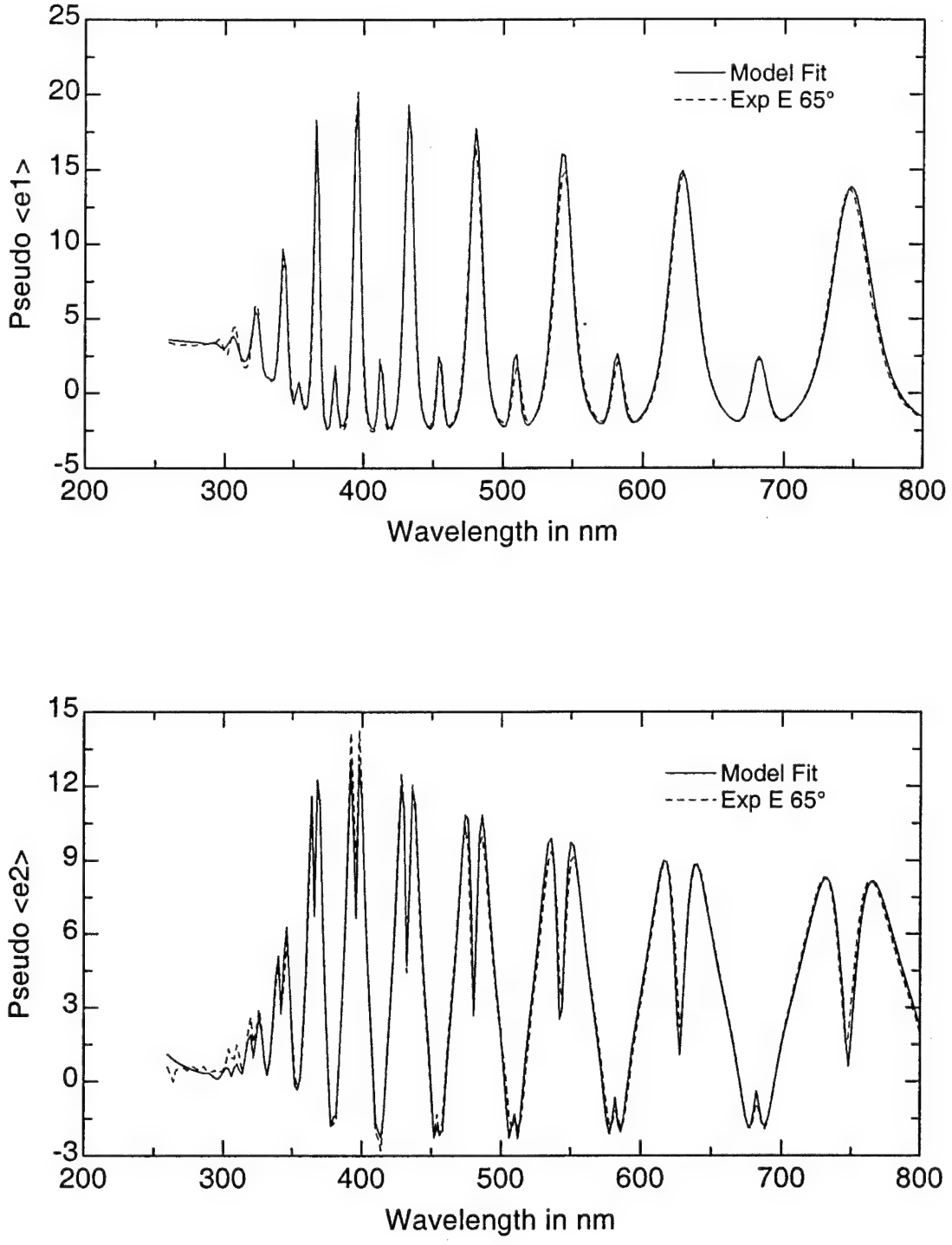

Figure 4-5. Fit to the 1400-27 sample.

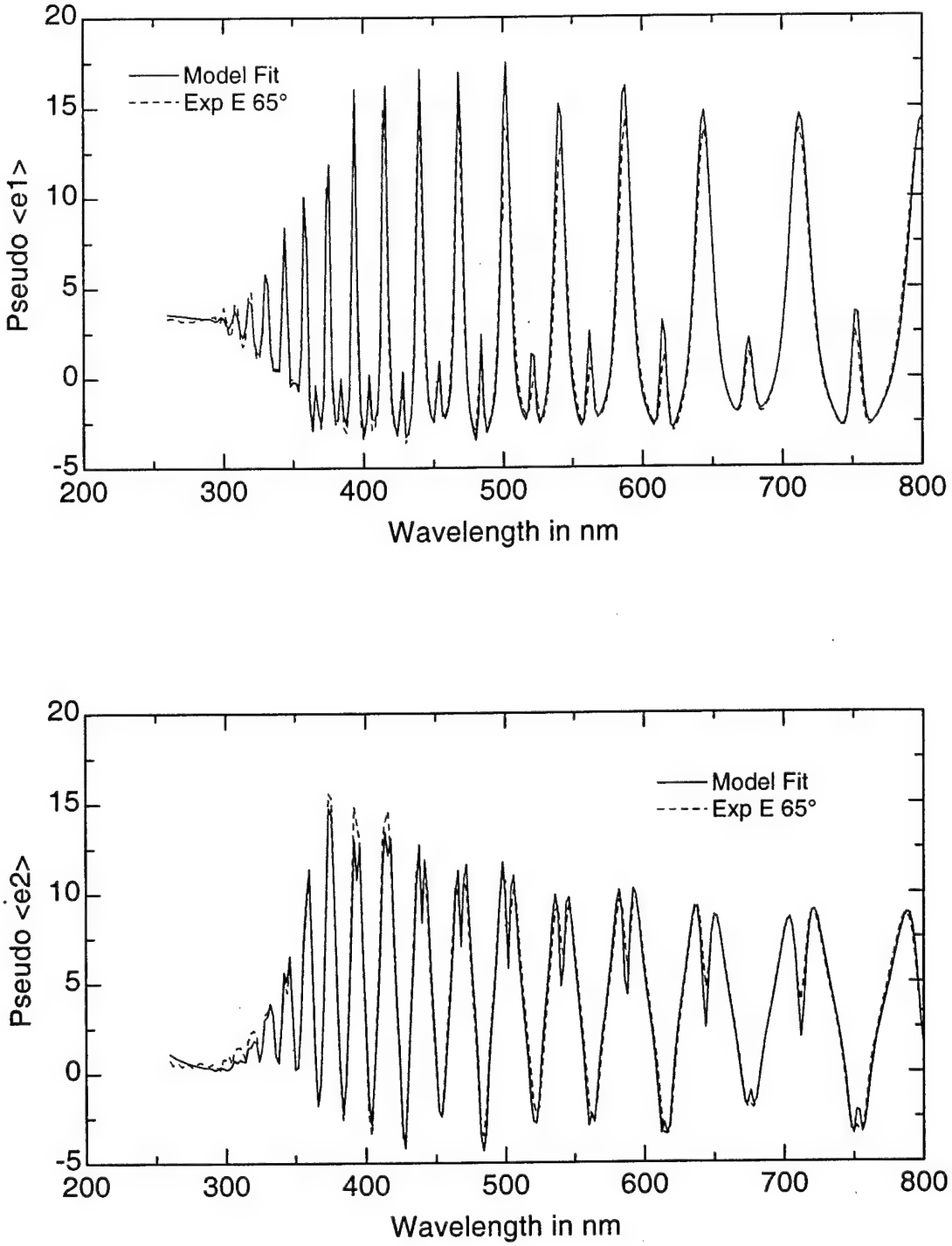

Figure 4-6. Fit to the 1400-27/PMGI two layer sample.

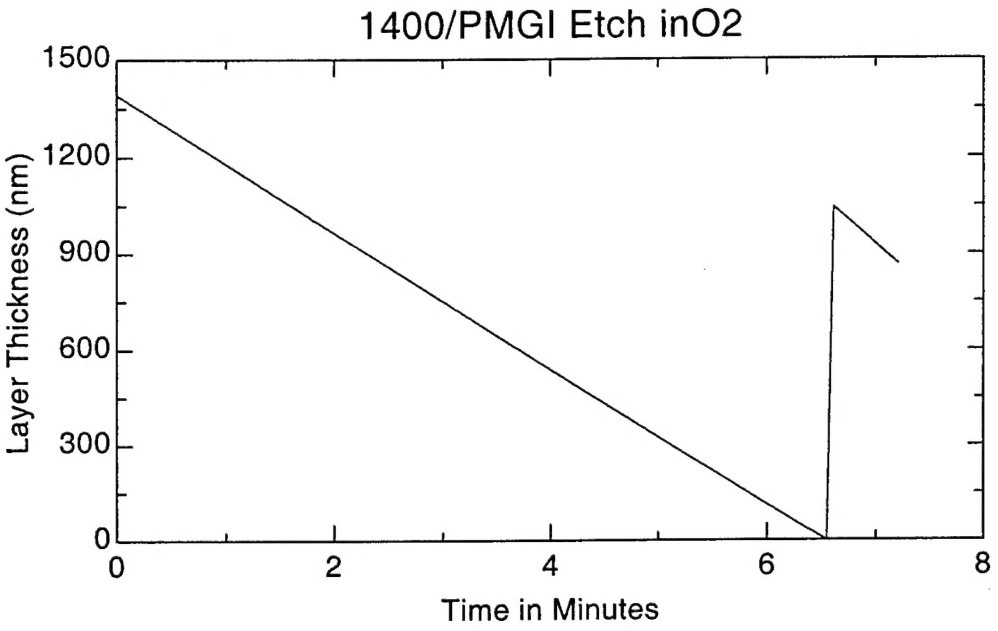

Figure 4-7. 1400-27 and PMGI layer thickness during control etch.

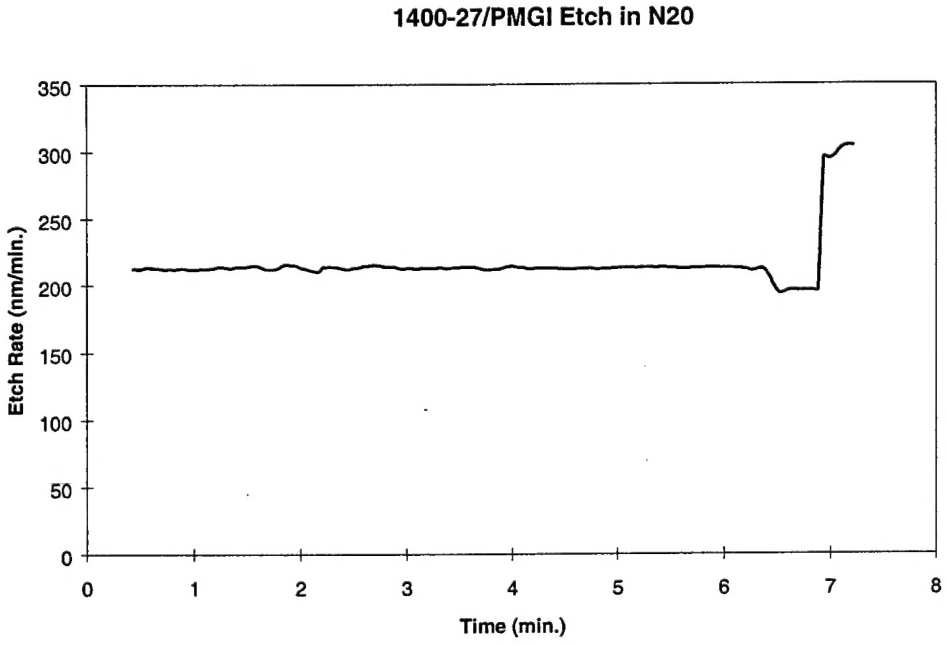

Figure 4-8. Etch rate during PR etch control run.

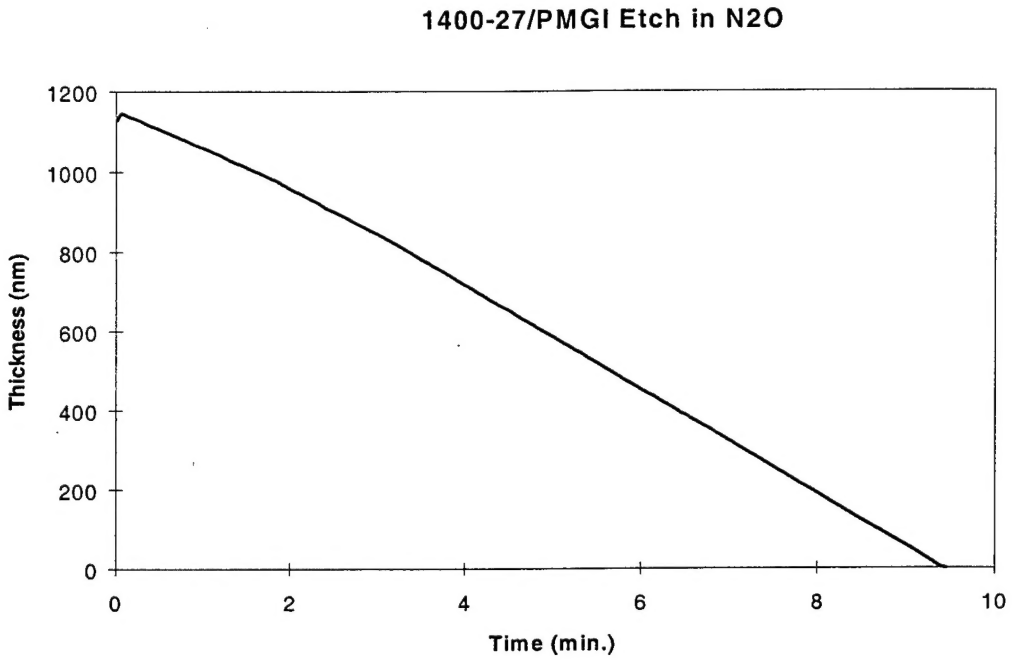

Figure 4-9. 1400-27 thickness during etch rate control run.

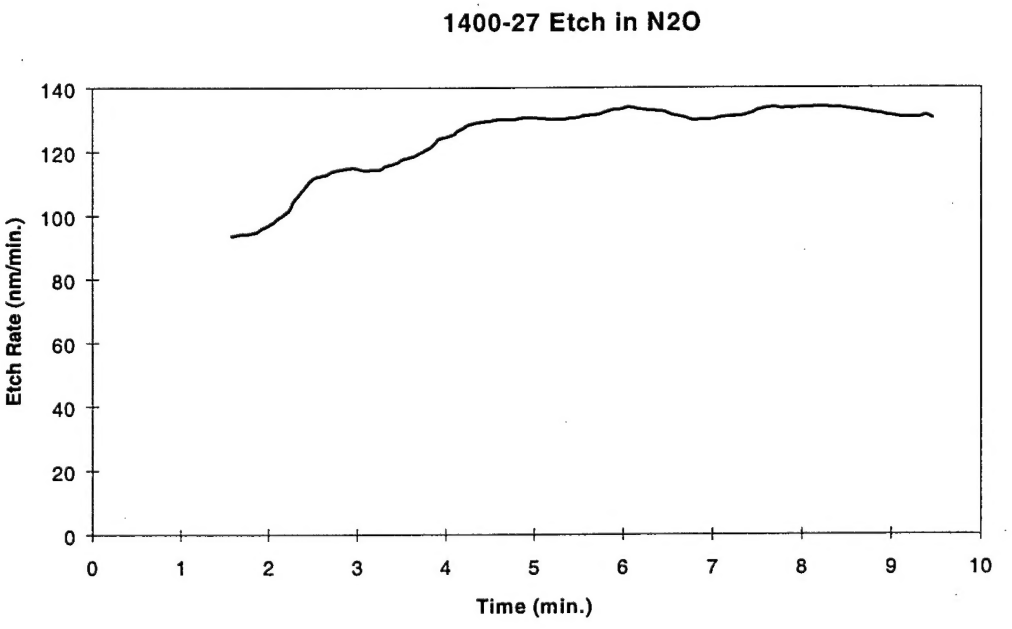

Figure 4-10. 1400-27 etch rate during etch rate control run.

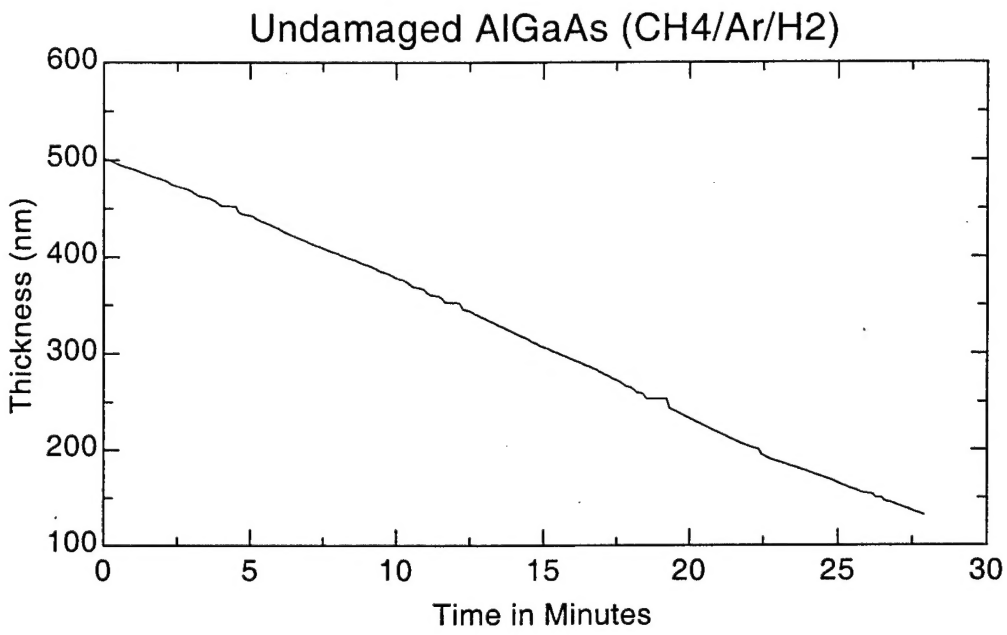

Figure 4-11. AlGaAs thickness during etch control run.

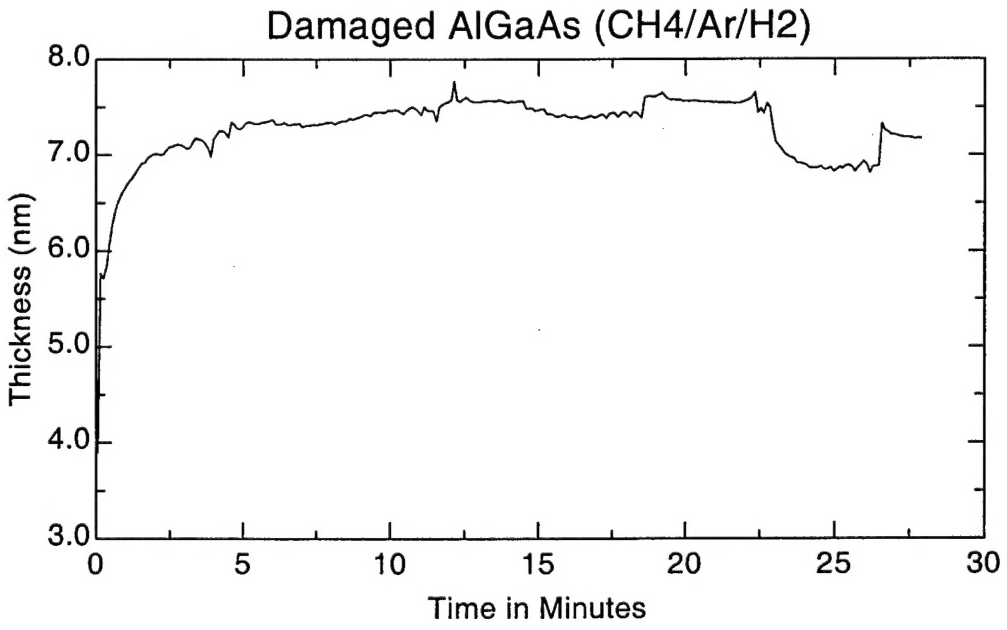

Figure 4-12. Damaged AlGaAs thickness during etch control run.

SUMMARY

Etch rate modeling of GaAs etched in a $CH_4/Ar/H_2$ ECR plasma with rf induced dc biasing of the sample was done empirically using Discovery and Optimization software from Int'l Qual-Tech, Ltd. The "design of experiments" approach was used with the process variables microwave power, bias voltage, and operating pressure. The generated model equation was

$$E = -1764 + 1.725M - 0.22MP + 32.8B - 0.13B^2 - 95.1P + 16.05P^2$$

where E is the etch rate in Å/min., M is the microwave power in watts, P is the pressure in millitorr, and B is the rf induced dc bias in +volts. This equation predicts the etch rate for any level of the variables within the investigated range of each variable. These ranges were: microwave power, 100 to 300W; bias, -75 to -150V; and pressure, 1 to 5 millitorr. The 95% confidence for the model predicted values was ±180 Å/minute. A response surface plot of the predicted etch rate as a function of the process variables was generated by Optimization. From the plot, the optimum operating point (the variable levels which produce the maximum etch rate) was determined to be 300W microwave power, -128V bias, and pressure of 1 millitorr.

Etching of GaAs and AlGaAs samples with a $CH_4/Ar/H_2$ ECR plasma resulted in an etch induced surface damage layer for both materials. Additional GaAs samples were etched in pure H_2 and pure Ar plasmas and analyzed using *ex-situ* VASE and AES. The damage was identified as a thin, strained layer caused by the preferential removal of As by hydrogen in the near surface region. *In-situ* data from $CH_4/Ar/H_2$ etching of GaAs and AlGaAs were used to optically model the damage. The thickness of the damage layer for each material was found to be ~15 nm for GaAs and ~12 nm for AlGaAs.